Electrochemical Performance and Failure Mechanism of Phosphorus/Graphite Composite as an Anode for Na-ion Batteries

Yongil Kim

Department of Energy Engineering

(Battery Science and Technology)
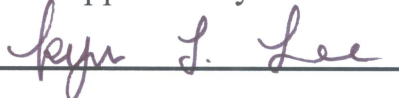
Graduate School of UNIST

2015

Electrochemical Performance and Failure Mechanism of Phosphorus/Graphite Composite as an Anode for Na-ion Batteries

A thesis/dissertation

submitted to the Graduate School of UNIST

in partial fulfillment of the

requirements for the degree of

Master of Science

Yongil Kim

12. 18. 2014

Approved by

_____

Advisor

Kyu Tae Lee

Electrochemical Performance and Failure Mechanism of Phosphorus/Graphite Composite as an Anode for Na-ion Batteries

Yongil Kim

This certifies that the thesis/dissertation of Yongil Kim is approved.

12. 18. 2014

Signature

Thesis supervisor: Kyu Tae Lee

Signature

Nam-Soon Choi

Signature

Yoon Seok Jung

Abstract

These days, there are large applications of lithium ion batteries (LIBs) as energy conversion and storage devices, from portable devices (e.g. mobile devices) to large scale energy storage devices (e.g. power devices – electrical vehicles (EVs), military parts, and stationary electrical energy storage systems – energy storage system (ESS)). As expanding applications of the LIBs, the amount of demanding the LIBs is growing fast. But lithium reserves are not so much in Earth's crust and distributed in limited locations. Therefore, in the not too distant future, lithium prices will be raised inevitably.

At this point in time, Na-ion batteries (NIBs) are re-spotlighted and nominated for one of the post LIBs. The NIBs have typical two advantages of cost reduction. One is that sodium resources are abundant materials in Earth's crust. The other is that using Aluminum current collector is available on the anode for NIBs. However, at the present time, there are limitations for practical using NIBs. Many materials for NIBs have not been developed up to now. On the cathode materials, comparing with cathode materials for LIB, the cathode materials for NIBs have lower operating voltage and lower specific capacity. And on the cathode side, it has limitations for the intercalation chemistry. Hence, the development of the anode materials for NIBs should be conducted. Among them, the anode materials for NIBs should have lower operating voltage and higher specific capacity to increase energy density for NIBs.

In this situation, an amorphous red phosphorus/carbon composite was introduced as a promising anode material for NIBs. Because the red phosphorus has poor electronic conductivity, the carbon acts as a conductive material. It showed the highest reversible capacity and suitable operating voltage for NIBs. But the composite has poor cycle-ability in terms of long cycling. Because alloying compounds (in this case, phosphorus) have severe volume expansion and shrinkage that cause contact loss, and then capacity fading is happened. The carbon couldn't sufficiently act as a buffer matrix in this case.

Therefore, to improve cycle-ability for phosphorus composite materials, a new composite structure is adopted and an electrolyte additive is used in this research. Firstly, a phosphorus/graphite composite is used as an anode material for NIBs. The composite is obtained via a facile and simple mechanochemical ball milling process. The composites are tested by two kinds of different weight ratio. The two composites show that high reversible

capacities and good cycle-ability comparing with previously reported the amorphous red phosphorus/carbon composite. And by having different graphite contents, the two composites have different structures which affect the reversible capacity, the cycle-ability, low changing ratio of electrode thickness, surface area, and pore volume. Hence, optimizing weight ratio of the phosphorus/graphite composite, higher reversible capacity and good cycle-ability can be achieved simultaneously. Secondly, fluoroehtylene carbonate (FEC) is used as an electrolyte additive, surfaces of electrodes and Na metals are analyzed. The FEC used case shows better electrochemical performances than the FEC unused case. To define different points between the two cases, EIS and XPS analysis are carried out on the electrodes and the Na metals. In EIS result, charge transfer resistances have different behaviors between the electrodes and the Na metals. To investigate these phenomena, XPS analysis is conducted, and the XPS result shows that compositions of solid electrolyte interphase (SEI) layers and surface are different between the cases. The FEC additive makes stable SEI layers and minimizes oxidation of phosphorus on the electrode.

Through the results in this research, the phosphorus/graphite composite can fulfill increasing electronic conductivity and buffer matrix structure. Phosphorus is coated by graphite, exposure of phosphorus is minimized. And the composite can be one of the promising anode materials for NIBs by having high reversible capacity and low operating voltage. Additionally, using the FEC additive can further enhance the electrochemical performances by making stable surface for the composite.

Contents

List of figures

List of tables

Ⅰ. Introduction

Lithium ion batteries (LIBs) were first commercialized in 1991 by Sony. These devices have been one of the most efficient and fantastic energy storage devices. Currently, they are used for various purposes, portable devices, electric vehicles, military materials, and energy storage systems (ESS). Lithium ion batteries for portable devices have been widely used from old times, present directions go toward electric vehicles and energy storage systems. Electric vehicles consist of large-scale lithium ion batteries that are source of power. In the automobile market, electric vehicles parts are increasing attention and have been developed. Electric vehicles market should not only be gotten more attention, but also make a bigger pie for automobile market. Furthermore, LIBs are currently being developed and being used for electrical energy storage (EES).[1-5] Then, the key element of LIBs is lithium absolutely. The lithium element is existed in the mother Earth's crust. But the lithium element is not an abundant element, compared with other elements. Also, markets which are based on LIBs are growing fast in existence applications and the increasing demands for LIBs cause the increasing cost of materials based on LIBs. Additionally, lithium reserves have limited amount and are distributed uneven locations. Here, the sodium element is one of the alternative key elements. The sodium element and sodium based precursors are abundant resources, because the sodium element is one of the most abundant elements in the Earth's crust (6th) and there are many possible extraction methods getting the sodium in the sea water representatively. Additionally, the sodium is the same group (alkali metal) with the lithium in the periodic table. It implies that the sodium based chemistry can be applied into the lithium based chemistry. But there are different chemical and physical properties compared with the lithium.[6-8]

Sodium ion batteries (NIBs), like LIBs, are widely interesting research parts in the energy conversion and storage system currently. The NIBs researches are rapidly growing in the field of electrode active materials, sodium salt based electrolytes, their own characteristic properties, and so on. Especially, NIBs are a potential candidate for the practical useable EES, because the sodium based material is abundant and low cost for large-scale applications. Especially, cheap Al current collector can be used on the NIBs anode. Although energy density of NIBs is lower than that of LIBs, it can be solved by increasing size for the stationary large-scale EES. Currently in NIBs, many NIBs cathode materials were researched

and were based on intercalation chemistry. But, in terms of NIBs anode materials, some NIBs anode materials were studied and high capacity NIBs anode materials have not been researched enough.[6-8]

To get the high capacity anode, the anode active materials should have conversion reactions or alloy reaction, or both of them. But they suffer from severe capacity fading phenomena. To overcome severe capacity fading problems and get a long cycle-ability for the batteries, the choice and development of active materials, modified structures for active materials, electrolytes, additives, binders, and modified formation of solid electrolyte interphase (SEI) layers should be conducted.[9] These solutions are helpful to solve problems and approach possible breakthroughs for the high capacity anode materials.

Currently, our group demonstrated the electrochemical performance of the amorphous red phosphorus/carbon composite as a promising anode material for NIBs. Here, the amorphous red phosphorus/carbon composites showed excellent electrochemical performance for NIBs. These amorphous red phosphorus/carbon composite powders were obtained via a facile and simple ball milling process using commercially available amorphous red phosphorus and Super P carbon with a weight ratio of 7:3. The composite delivered the highest reversible capacity, 1890 mA h g^{-1}, among any reported anode materials for Na-ion batteries.[10]

In this study, we try introducing the phosphorus/graphite composite which shows a unique structure which is different from previous amorphous red phosphorus/carbon composite. Difference of two composites is that the amorphous red phosphorus/Super P carbon composite has one dimensional linkage between phosphorus and carbon which can be called dotted contact. On the other hand, the phosphorus/graphite composite has two dimensional linkages between exfoliated graphite and phosphorus which can be called planar contact. The characteristic structure of planar contact helps to maintain more stable active material state and be expected to keep the longer cycle life.

Also, we investigate different weight ratio effects for the phosphorus/graphite composite and failure mechanism of the phosphorus/graphite composite. Finally, we research effects of fluoroethylene carbonate (FEC) electrolyte additive for the phosphorus/graphite composite.

Ⅱ. Literature research

2.1 Introduction and operation principle of Li-ion batteries (LIBs) and Na-ion batteries (NIBs)

The initial lithium secondary batteries were used lithium metals for anode materials. But, several problems were happened. Representatively, reversibility of the lithium metals is low and the lithium metals cause safety issues. At the charging processes, lithium ions which are solvated in the electrolyte are reduced on the lithium metal anode and develop like dendritic formations. The dendrite lithium metal is grown sharply, so the structure can be broken easily and be in existence like losing electrical conductivity (dead volume state). Otherwise, in case of the grown dendrite lithium metal too lengthy, the dendrite lithium metal can pass through the separator and cause short circuit by touching the opposite electrode. The short circuit gives rise to very big current, then some resistance parts can generate heat and flammable agents accompany explosion. This dendrite growth is remarkable in case of high current density, the quick charging and discharging situation can affect safety problems fatally.

Although the lithium metal is one of the lowest reduction potential which merits high energy density, safety issues hinder using the lithium metal as previously stated. To solve safety problems, two electrodes which can react with lithium ion and have lithium ion reversibly acceptable structures are considered instead of using the lithium metal electrode. In 1991 by Sony, these ion secondary batteries were first commercialized using carbonaceous materials for anode and lithium cobalt oxide ($LiCoO_2$) for cathode. These ion secondary batteries are called lithium ion batteries (LIBs), LIBs can store energy by shuttling lithium ions between cathode and anode reversibly without using the lithium metal electrode.

LIBs systems need to have electrochemically lithium intercalate/deintercalate-able anode and cathode materials, and electrolytes which can act as medium for lithium ions. Electrolytes are used by composing solvated lithium ion salts and non-aqueous solvents. Generally, cathode materials which include lithium ions and have reversibly lithium ion intercalate/deintercalate-able structures are considered. In the charging state, deintercalated lithium ions from the cathode go through the electrolyte and react with the anode. On the other hand, in the discharging state, deintercalated lithium ions from the anode go through the electrolyte and react with the cathode. Like these, lithium intercalate/deintercalate-able

materials are selected as the cathode and the anode, lithium transition metal oxide (lithium cobalt oxide) for the cathode and graphite for the anode are widely used.

In the charging state, lithium ions from the cathode go to the anode and voltage of battery is increased. And in the discharging state, lithium ions from the anode go to the cathode and the discharging reaction is happened spontaneously. In the reversible these processes, energy can be converted and stored, then used. Schematic diagram of operation principle in LIBs is described in Figure 1.[1]

In the same manner, same operation principle is applied to NIBs. Only, it makes an exchange with alkali cations.

Recently, NIBs have more attentions as alternative and post LIBs. The Sodium element compared with the lithium element is abundant in the Earth's crust. It induces a better competitive price than the lithium element. The sodium is the same group (alkali metal) with the lithium in the periodic table. It implies that the sodium based chemistry can be applied into the lithium based chemistry. Therefore, development for NIBs can apply into the LIBs technologies (synthesis methods, material analysis, and in the research aspects) which have been developed for decades. Also possibility of commercialization for NIBs is higher than the other post LIBs.

Additionally, because of the bigger size sodium ion than the lithium ion, this characteristic can give rise to opportunity of various materials design. The different degree of ionic radius between the sodium ion and the transition metals is bigger than that of between the lithium ion and the transition metals. That point can give possibility of various materials design. And based on mineralogy database, there are many minerals composed of the sodium ions. The sodium ion case has more than the lithium ion case for the many minerals with various crystal structures formed thermodynamically stable phases in the Earth. Moreover, the sodium ion has lower desolvation energy in the electrolyte because of bigger size.[11]

However, comparing with the lithium ion, the larger sodium ion may cause poorer kinetics than the lithium ion. Also, the heavier sodium ion and the higher reduction potential sodium ion affect the lower energy density than the lithium ion. And because of different thermodynamically stable phases between the sodium and the lithium, the NIBs can't apply into the LIBs technologies perfectly.

Therefore, many researches and developments are needed about various materials and mechanisms for NIBs systems.
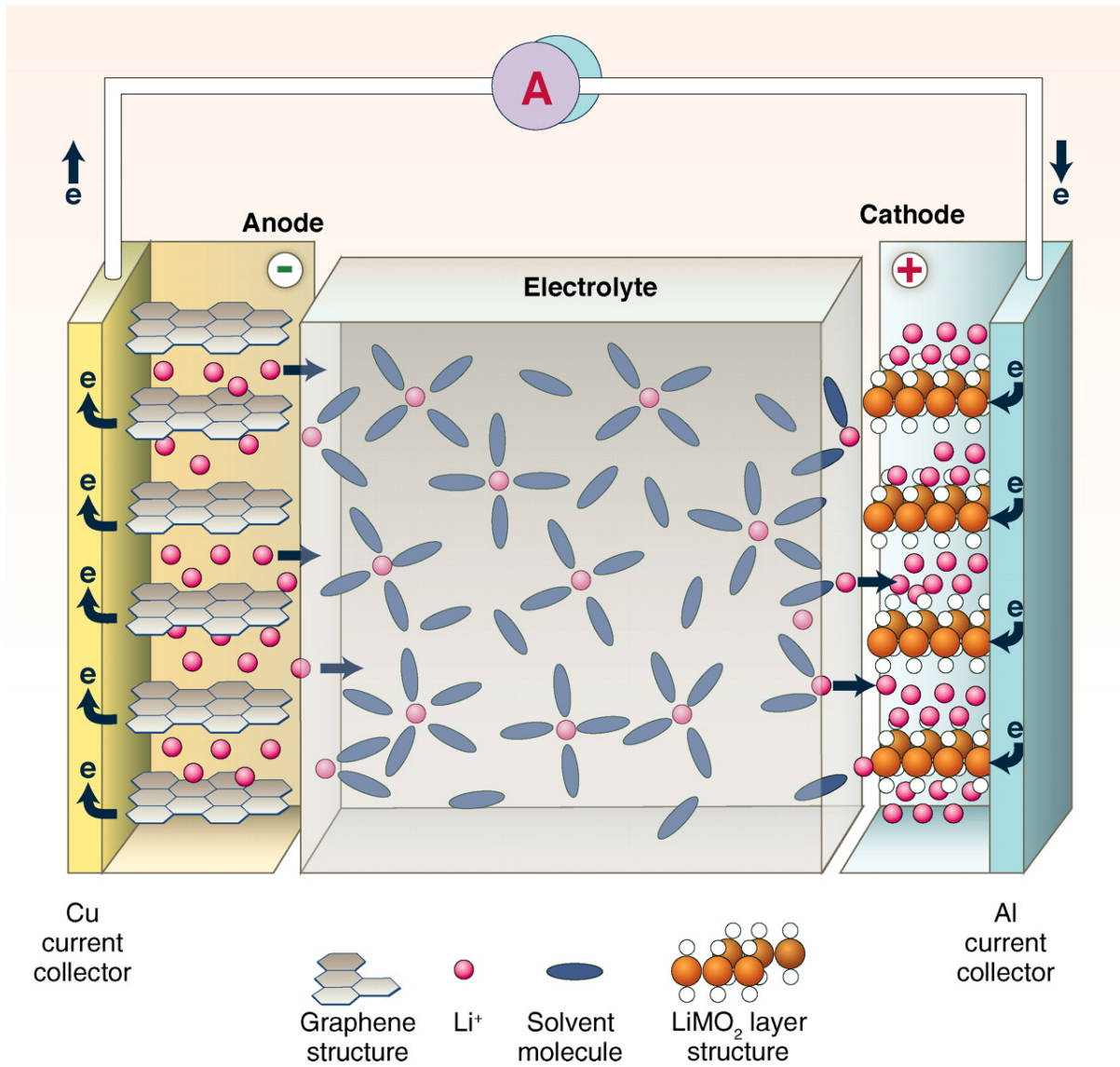
Figure 1. Schematic diagram of operation principle in LIBs

2.2 Components in sodium ion batteries

Like as LIBs, NIBs are operated by reversible shuttling Na ions between the anode and the cathode. Because of the operating principle, the anode and the cathode should be used as sodiation/desodition-able materials, and the cathode materials can generally deinsert the Na ions in charging process. In other hand, the anode materials can commonly insert the Na ions in discharging process. And, as a medium which is able to conduct the sodium ions, electrolyte which is composed of soluble Na salts and nonaqueous solvents is used. Lastly, to prevent directly physical and electronic contacts between two electrodes, separator which is composed of polymer films is used. There are many parts as the components in the NIBs. Among them, 4 parts (cathode, anode, electrolyte, and separator) are representative. Therefore, to perform a battery, all the components should fulfill their roles.

2.2.1 Anode materials

Anode materials for NIBs can be classified by three different reaction mechanisms observed in electrode materials same as LIBs. Three different reaction mechanisms are composed of insertion, alloying, and conversion. Among them, intercalation compounds are the most common negative electrode material used in current LIBs. But in NIBs, only a small amount of Na can be stored in graphite. And typical intercalation compounds for NIBs are hard carbon. Also it can't perform enough capacity.

Therefore, to get high capacity, alloying compounds and conversion compounds have been considered as anode materials for NIBs. Alloying compounds are commercializing in LIBs. They can have very high capacity, but volume changes are severe. And conversion compounds have been developed (under R&D). Also, they can have high capacity, but voltage polarization causes decreasing energy density. Currently researched and developed anode materials for NIBs are described in Figure 2a.[11]

In Figure 2b,[11] the sodium can insert into the Group 14 and the Group 15 elements, and the alloy reactions are happened and formed binary compounds with Na. These elements interact with more than one mole of Na ions. These reactions can achieve high capacity than hard carbon anode material which have 300 mA h g^{-1} and is applied to intercalation chemistry. Then, there are big challenges that these elements have alloy reactions cause the large volume

expansion and shrinkage which affect cycle-ability, efficiency, and rate capability badly. Currently, many researches have been conducted to optimize these elements controlling compositions, structures, electrolytes, additives, binders, and so on. Additionally, Ceder's group[12] suggested that Na-based alloy materials have significantly low volumetric energy density compared with Li-based alloy materials. And Na-Me (Here, Me = Si, Ge, Sn, and Pb) alloy materials are limited to numbers compared with Li-Me alloy materials, because of different kinetics and thermodynamics between Na and Li. Among them, representative mono materials are Sn,[13-15] Sb,[16-18] and P.[10,19] When fully sodiated each of them, Sn forms $Na_{15}Sn_4$, Sb forms Na_3Sb, and P forms Na_3P theoretically. These materials also optimized by electrolytes, additives, and binders and have been researched now days.

And conversion compounds for NIBs can be divided by 4 kinds. These are metal oxide, metal sulfide, metal selenide, and metal phosphide. At this metal, the metal doesn't react with Na ions. An example of compound is NiP_3.[20] Theoretically, one mole of phosphorus can react with three moles of Na ions and the others can react with two moles of Na ions.

Lastly, there are materials which can have both the alloy reaction and the conversion reaction. These materials are composed of metals which can react with Na ions (alloying compound). They are also composed of metal oxide, metal sulfide, metal selenide, metal phosphide, and multiple compounds. Representative materials are SnSe,[21] SnSb,[22,23] Sn_4P_3,[24] and so on. Additionally, more than binary, ternary materials are possible.[25] In here, tin phosphide showed excellent electrochemical performance for NIBs, delivered a reversible capacity of about 700 mA h g^{-1} and exhibited very stable cycle performance with a negligible capacity fading over 100 cycles. And tin phosphide has the highest volumetric specific capacity and good electrical conductivity without a conductive material.[24] Most of binary materials have a typical one's strength that one of them acts as a buffer matrix, this phenomenon improve stability of electrode materials.[26,27] These binary materials also enhanced by electrolytes, additives, and binders and have been developed recently. Designing and maintaining better high capacity NIBs anode, electrolytes, additives, and binders are essential parts. Choosing and modifying suitable electrolytes, additives, and binders make stable and moderate solid electrolyte interphase (SEI) layers. Therefore, making better SEI layers is one of the most important key to commercialize the high capacity LIBs and NIBs. Followed by reference papers are required conditions for the high capacity anode, especially NIBs.[9,13-15,22,23,26,28-32]
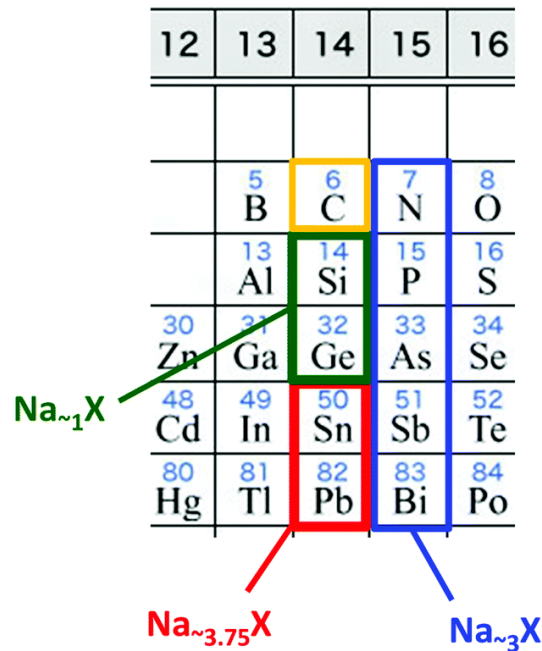
a)
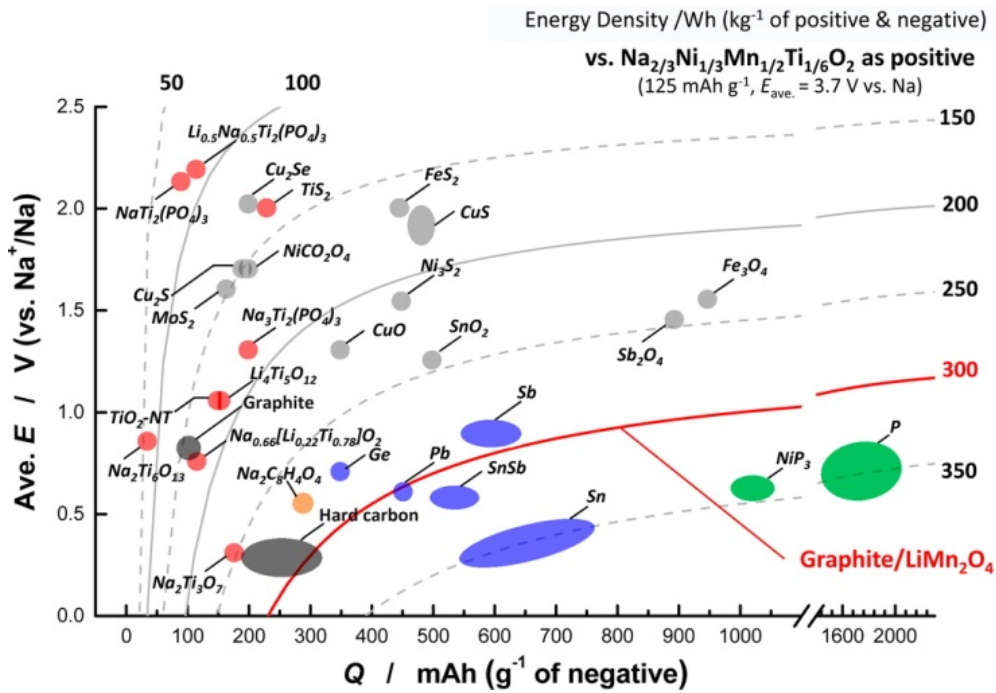
b)

Figure 2. Anode materials for NIBs: a) voltage-capacity and energy density-capacity plots b) formation of binary compounds with Na

2.2.2 Cathode materials

Up to now, many cathode materials have been researched based on intercalation chemistry (Figure 3[11]). Category of cathode materials for NIBs can be divided by four kinds. There are transition metals layered oxides, other sodium intercalate-able transition metals oxides, polyanionic compounds, and the others sodium intercalate-able materials.[11]

In case of the layered oxides, reversible sodium intercalate-able transition metal oxides were researched by Delmas in the early 1981.[33] Because of concentration for LIBs technologies, research for NIBs was excluded for decades. But in these days, research for NIBs has been re-spotlighted as one of the post LIBs technologies. And the thermodynamic properties and the kinetically properties of Na ions are different from those of Li ions, they cause making different structure and showing different properties. For example, $LiFeO_2$ can't be directly synthesized, because Li^+ and Fe^{3+} have similar sizes that cause cation disordering and making rock salt structures. On the other hand, $NaFeO_2$ can be synthesized directly. And Na_xCrO_2 has reversible capacity comparing with $LiCrO_2$ by having different size of sites and forming energetically stable transition metals (Cr^{6+}, Cr^{4+}) in Na_xCrO_2.[34] Through these size effects, $NaNiO_2$, Na_xVO_2, $Na[Ni_{1/2}Ti_{1/2}]O_2$ are introduced.[35-37] Representative example of the layer oxides is $Na_{2/3}[Fe_{1/2}Mn_{1/2}]O_2$, in this material, sodium ions can be easily ionized than lithium ions case, resulting in having the lower covalent bonding with oxygen. In other words, iron and oxygen can have more electron density than lithium case. Then, the redox potential of the Fe^{3+}/Fe^{4+} is lower than lithium case, resulting in having electrochemical performances without oxygen loss and can be used as a relatively high operating voltage in NIBs.[38] And in case of the polyanionc compounds, typical examples of these compounds are phosphate ions based materials like as LIBs case.[39,40] Representative example of the phosphate compounds is $Na_2FeP_2O_7$.[41]

Therefore, to design novel cathode materials for NIBs, we should know differences between the Na cases and the Li cases. Then, we can find breakthroughs to forward increasing energy density for NIBs.
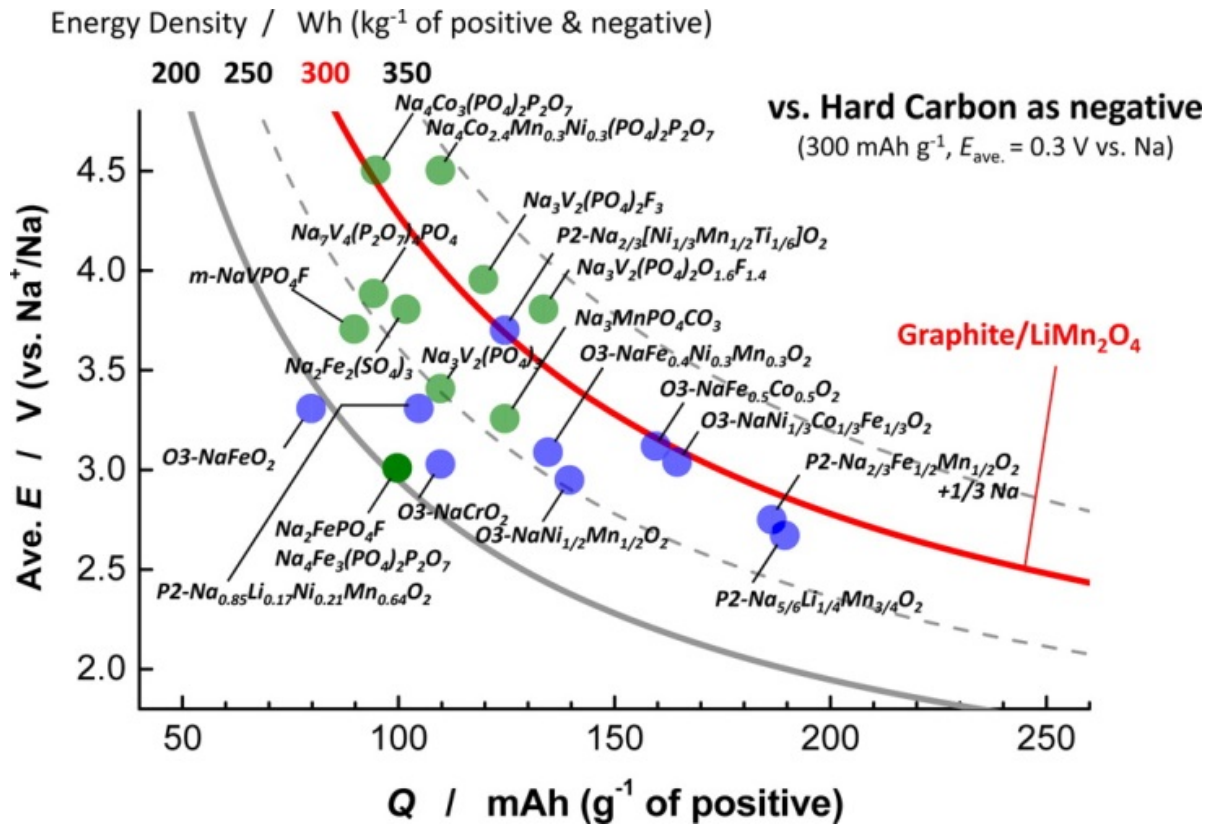
Figure 3. Voltage-capacity and energy density-capacity plots of cathode materials for NIBs

Ⅲ. Experimental

3.1 Active material preparation

The composite was prepared by a mechanochemical ball milling using a planetary ball milling machine (Pulverisette 6, Fritsch). The pristine graphite (Natural graphite, 100 mesh (< 150 um)) and red phosphorus were put into a silicon nitride ball milling container containing silicon nitride balls (diameter for 5 mm). The synthesis method and the weight ratio of the composite are described in Figure 4 and Table 1. The container was aeembled under an Ar atmosphere. The container was agitated at 500 rpm for 24 hours.

3.2 Electrode preparation

Samples of electrochemically active materials were mixed with carbon black (Super P) and Polyacrylic acid (PAA) binder in a 7:1:2 weight ratio.

3.3 Electrochemical characterization

The electrochemical performance was estimated using a two-electrode 2032 coin-type half-cell, where Na metal was used as the counter electrode. The working electrode was spot-welded to the bottom (Case) of the coin cell. The mass loading of the electrodes is about 1~2 mg cm^{-2}. Galvanostatic charge and discharge cycling (WonATech WBCS 3000 battery measurement system) was carried out in the potential ranges from 0.0 to 2.0 V vs. Na/Na$^+$. The cycling retention performance of the half cells was evaluated at a current density of 200 mA g^{-1} at 30℃. To investigate the rate performance of the half cells, capacities were measured at the current densities of 0.1, 0.2, 0.4, 0.6, 1.0, 2.0, and 4.0 A g^{-1} at 30℃. For electrochemical impedance spectroscopy (EIS) measurements were evaluated by Biologic (SP-150). The electrolyte solutions were composed of 1.0 M NaClO$_4$ in a mixture of ethylene carbonate (EC) and diethyl carbonate (DEC) (50:50, v/v) solvent with or without 5 wt. % fluoroethylene carbonate (FEC, Soulbrain Co. Ltd.). Microporous polyethylene film was used as a separator. Cells were assembled in an Ar-filled glove box with less than 1 ppm of both

oxygen and moisture.

3.4 Material characterization

Powder X-Ray diffraction (XRD) data were collected on a Rigaku D/MAX2500V/PC powder diffractometer using Cu-Kα radiation (λ = 1.5405 Å) operated from 2θ = 10 – 80˚. The shape and structure of composite material were examined by a scanning electron microscope (SEM; S-4800, Hitachi) and the elements distribution of energy dispersive spectroscopy (EDS) mapping was examined by a high resolution transmission electron microscope (HR-TEM; JEM-2100F, JEOL). The cross section image and line profiling for element analysis using energy dispersive spectroscopy (EDS) were obtained by dual-beam focused ion beam (Dual-beam FIB; Quanta 3D FEG, FEI). Surface analysis was examined by XPS (Thermo Fisher). The N_2 adsorption and desorption isotherms were collected at 77 K with a Micrometrics ASAP 2420 Gas Adsorption Analyzer. The Raman spectra were obtained with a Micro-Raman (Raman; alpha300R, WITec).

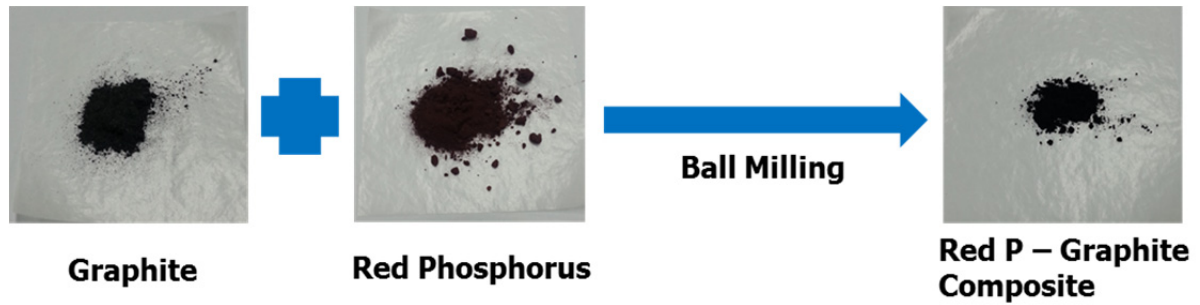**Figure 4.** Synthesis method diagram and abbreviation of two kinds of samples

Table 1. Abbreviations of the phosphorus/graphite composites

Weight of Red P	Weight of Graphite	Abbreviation
5	5	GP55
7	3	GP37

Ⅳ. Results and discussion

4.1 Analysis for the phosphorus/graphite composite as an anode for NIBs

4.1.1 The phosphorus/graphite composite

The phosphorus/graphite composite is prepared by simple mechanochemical ball milling synthesis method utilizing commercial amorphous red phosphorus and plate natural graphite with weight ratio of 5:5 (abbreviation for the composite is 'GP55') and 3:7 (abbreviation for the composite is 'GP37').

The SEM image of Figure 5a shows that the overall particles for the composite. The secondary particles have broad size distributions by the mechanochemical ball milling synthesis. The SEM image of Figure 5b shows that the primary particle size is about 100 nm. The secondary particle which is agglomerated of the primary particles size is about several micrometers.

The composite is composed of carbon, phosphorus, and oxygen mostly, as shown in the HR-TEM image and EDS mapping images of the composite for Figure 6. Also the EDS mapping images clearly show that carbon, phosphorus, and oxygen are distributed homogeneously based on a nanostructure. This resulting composite helps to improve electrical conductivity comparing with poor electrical conductivity red phosphorus.[10]

Additionally, the cross section image from Dual-beam FIB (Figure 7) shows that there are pore sites in the secondary particle. This structure can alleviate volume changes during processes of charging and discharging. From the line profiling graph in the cross section image (Figure 7), the graph shows that the particle is composed mostly of the carbon and the phosphorus with distribution homogeneously.

The composite is further examined by the Raman spectra as shown in Figure 8. The red phosphorus shows Raman peaks only for red phosphorus. But the composite can't be observed Raman peaks for red phosphorus, and only exfoliated graphite (graphene-like) peaks were showed at 1350 and 1584 cm^{-1} for D- and G- bands individually. The composite seems to be covered by exfoliated graphite on the red phosphorus, resulting in decreasing the intensity of the red phosphorus peaks.[10]

And the X-ray diffraction patterns of Figure 9 show that the red phosphorus has broad peak

patterns, and the phosphorus/graphite mixture has broad peak patterns of the red phosphorus and a strong sharp peak of 26.5° which demonstrates [002] directions and matches a d-spacing of 0.34 nm for graphite. The other peaks match the graphite pattern. But the GP55 composite and the GP37 composite show that they have broad peak patterns generally, and the peak for [002] directions at 26.5° isn't shown. These XRD patterns of two composites indicate that evident exfoliation of the well crystallized graphite and the amorphized red phosphorus. Moreover, the GP55 composite is more amorphized than the GP37 composite as comparing two composites for XRD patterns.

When the conventional ball milling technique is applied, the result of ball milled shows that the red phosphorus and the graphite are changed into the exfoliated graphite/amorphous red phosphorus composite. Therefore, the Raman peaks and the XRD patterns for the two GP composites indicate that the graphite is undergone an obvious edge distortion caused from the reduction of grain size by the conventional ball milling technique. The technique brings to the mechanochemical breaking off C-C bonds in the graphite.[42] Thus, the well crystallized graphite and the red phosphorus are amorphized, and the amorphized graphite envelop the amorphized red phosphorus forming the composite, then the composite derives decreasing the intensity of phosphorus and graphite peaks and patterns for Raman and XRD respectively.[10,42]
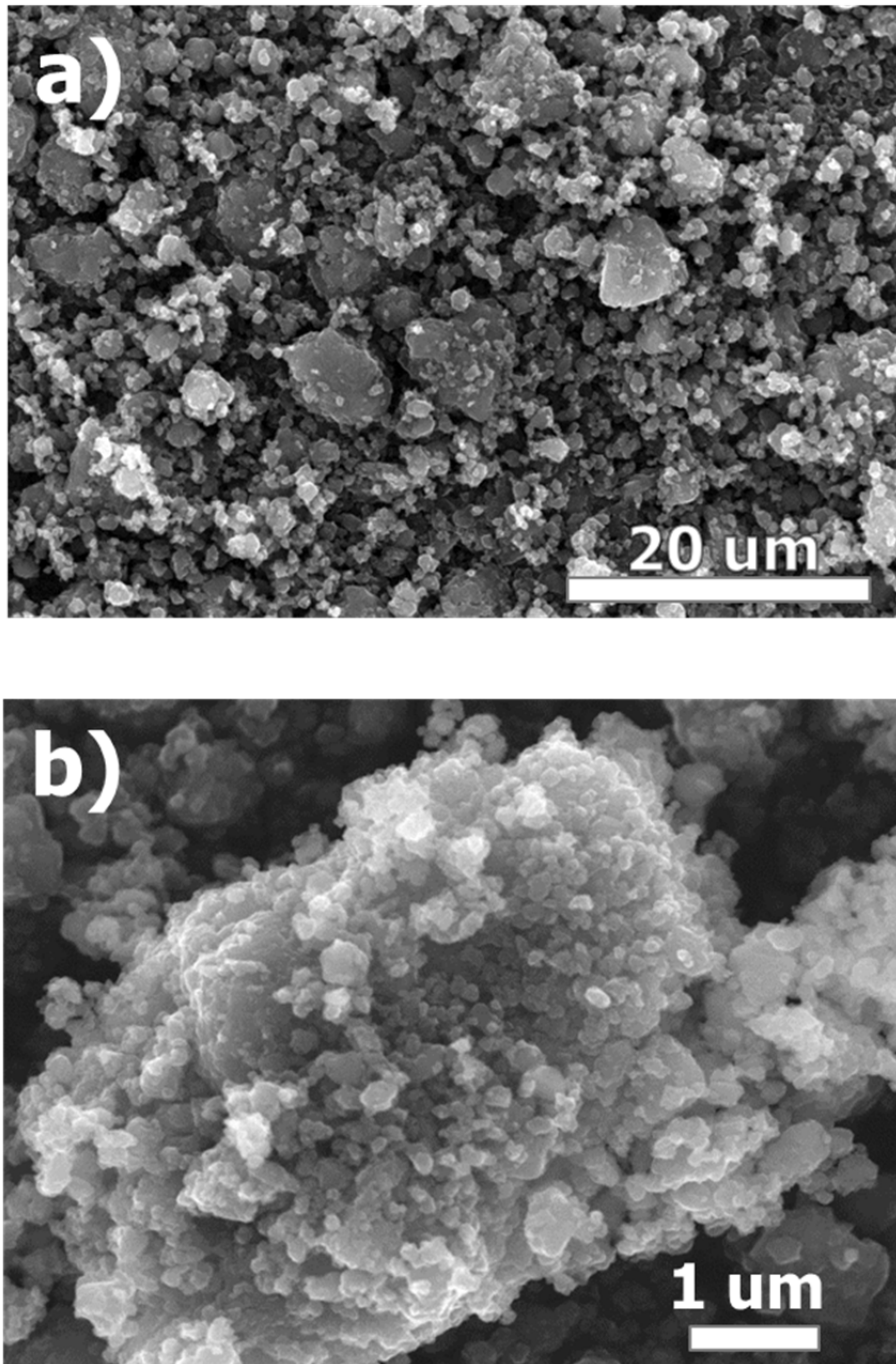
Figure 5. SEM images of the phosphorus/graphite composite: a) overall particles, b) a secondary particle
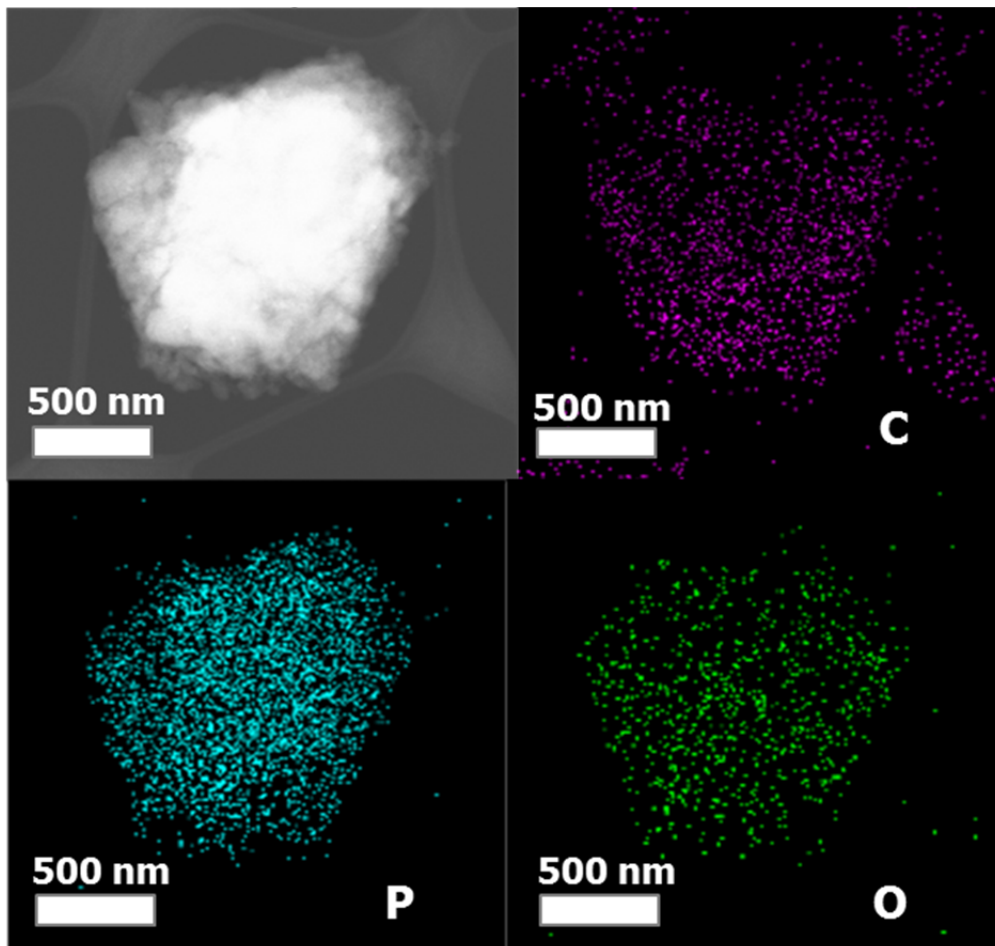
Figure 6. HR-TEM image and EDS mapping images of the phosphorus/graphite composite
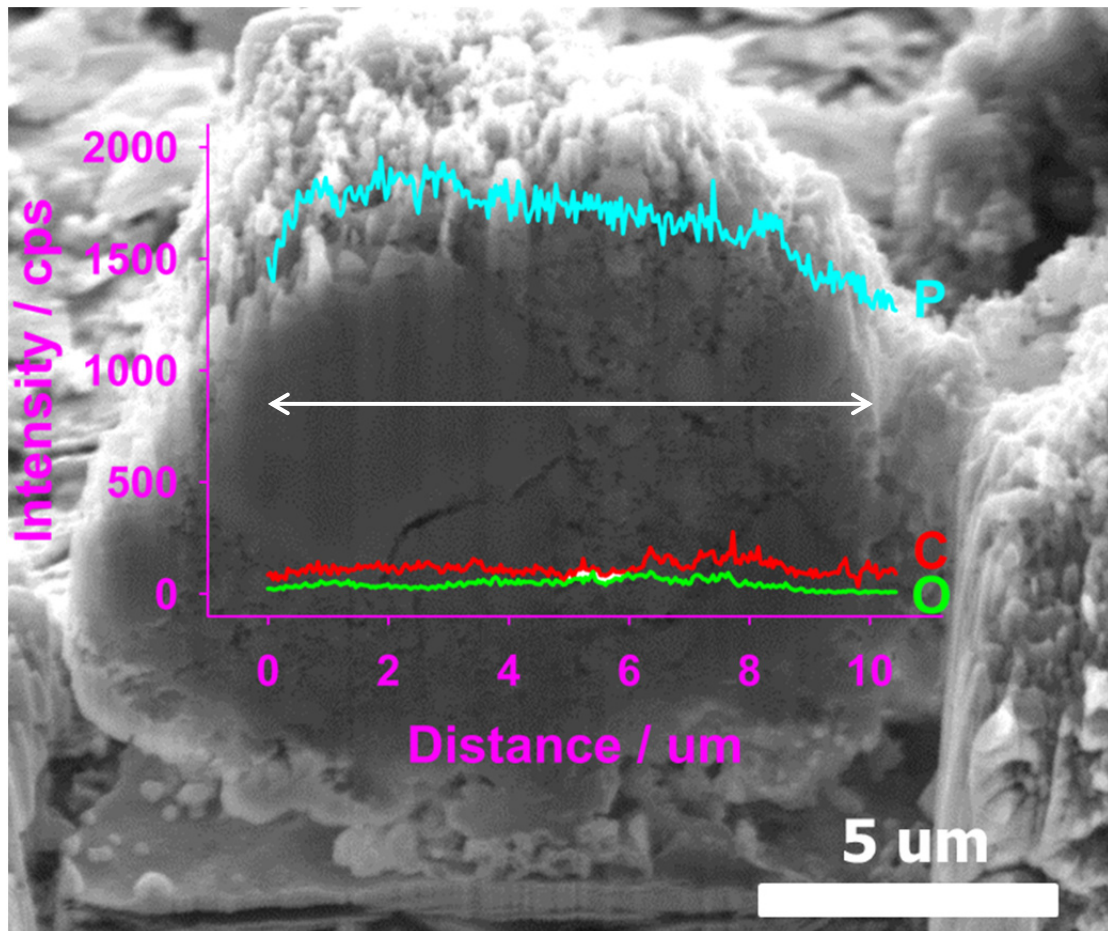
Figure 7. Dual-beam FIB image and EDS line profile graph (inside) of the phosphorus/graphite composite

Figure 8. Raman spectra of the phosphorus/graphite composite and the red phosphorus

Figure 9. X-ray diffraction patterns of the phosphorus/graphite composite (GP55, GP37), the red phosphorus, and the phosphorus/graphite mixture

4.1.2 The ratio effects for the phosphorus/graphite composites

To define the ratio effects for the two phosphorus/graphite composites (GP55, GP37), the electrochemical performances of the two composites are tested, that is a type of half-cell with a sodium metal as a counter and reference electrode at the same time. The ele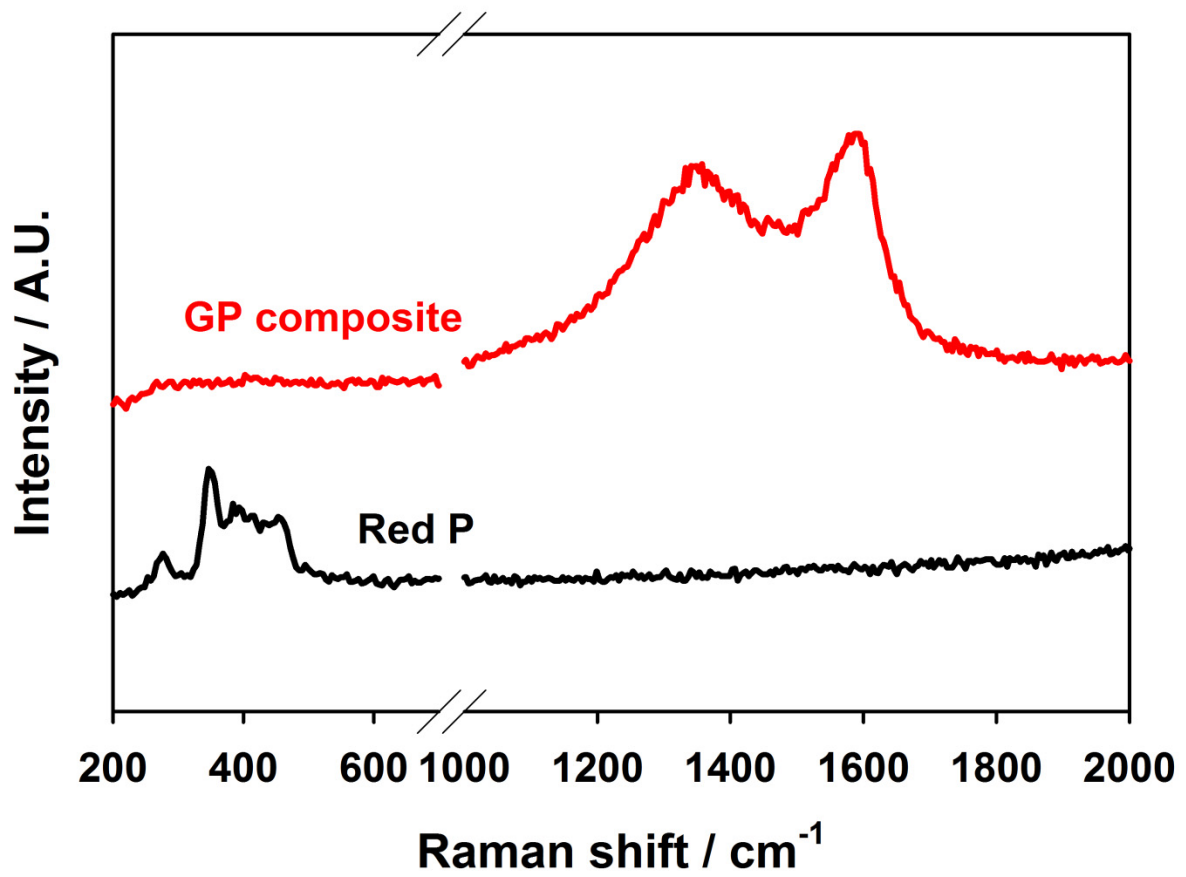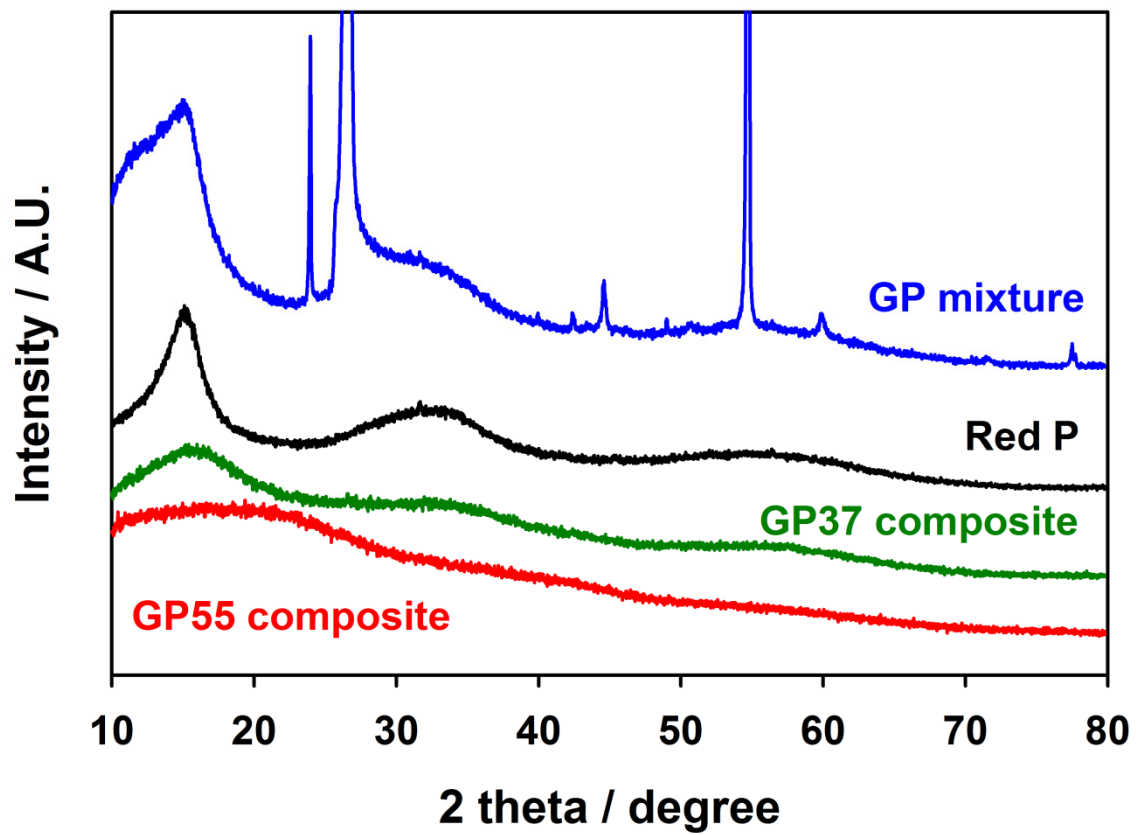ctrolyte of 1.0 M $NaClO_4$ / EC : DEC (v : v, 1 : 1) with 5 wt. % FEC (fluoroethylene carbonate, additive) is used for testing the two composites. Figure 10 shows the electrochemical performances that represent charge capacity (sodiation specific capacity) between 0.0 and 2.0 V at the constant current density of 200 mA g^{-1}. Comparing specific capacities between the GP55 composite and the GP37 composite, the GP55 composite shows 1480 mA h g^{-1} at the 1st cycle, 1375 mA h g^{-1} at the 50th cycle, and 1417 mA h g^{-1} at the 100th cycle. On the other hand, the GP37 composite shows 1688 mA h g^{-1} at the 1st cycle, 1669 mA h g^{-1} at the 50th cycle, and 334 mA h g^{-1} at the 100th cycle. Hence, the initial capacities of the GP37 composite are higher than those of the GP55 composite. But, the cycle-ability of the GP55 composite is better than that of the GP37 composite. In addition to, the both GP55 and GP37 composites have better cycle-ability than the CP37 composite which was amorphous red phosphorus/carbon composite and reported previously.[10]

Additionally, to confirm different structure effects between the GP55 composite and the GP37 composite, the ex-situ measurements of the electrode thickness are conducted. Figure 11 shows the voltage profiles of the GP55 and GP37 composites, and the thickness changes in electrodes during sodiation and desodiation are measured through the ex-situ measurements of the electrode thickness. The cells are disassembled and each of the electrode thickness is measured manually at various points indicated in the corresponding voltage profile. (1) pristine, (2) 0.2 V, (3) 0.0 V, (4) 0.8 V, (5) 2.0 V.[10] In case of the GP55 composite case, after full sodiation until the redox potential of the working electrode reached 0.0 V *vs.* Na/Na$^+$, the electrode thickness increased by 31%, which is lower than that in the GP37 composite case (52%). The electrode thickness change during sodiation and desodiation is reversible, and the initial electrode thickness is almost recovered with an expansion ratio of only 5.3% after full desodiation until the redox potential of the working electrode reached 2.0 V *vs.* Na/Na$^+$ in case of the GP55 composite. Otherwise, in the case of the GP37 composite, an expansion ratio of 15% is remained.

To distinguish a pore volume and a surface area between the GP55 composite and the

GP37 composite, the two composites are more analyzed by nitrogen adsorption/desorption (physisorption) analysis. The two composites have pore distributions of average pore diameter size from 30 to 60 nm (Figure 12a) mostly. And the two composites are measured by nitrogen adsorption/desorption isotherms (Figure 12b). The GP55 composite has the pore volume for 0.066432 cm^3 g^{-1} and the surface area for 11.9431 m^2 g^{-1}. Also, the GP37 composite has the pore volume for 0.050567 cm^3 g^{-1} and the surface area for 8.9214 m^2 g^{-1}. The two values of GP55 are higher than that of the GP37. (Table 2)

Therefore, putting together above results, the initial capacities of the GP37 composite are higher than those of the GP55 composite and the cycle-ability of the GP55 composite is better than that of that of the GP37 composite. In terms of initial capacities, because the ratio of graphite affects the electrode/electrolyte interface resistance, the high contents of graphite for the GP55 composite have the lower initial capacities than the GP37 composite.[43] And in terms of cycle-ability, generally, alloying compounds are undergone severe volume expansion and shrinkage during charging and discharging processes. Then, alloying compounds lose contact with the others and electrical conductivity. This process causes capacity fading after long-cycling. Hence, we apply the graphite which acts as helping electrical conductivity and supporting buffer matrix structure alleviating volume changes. And the GP55 composite has more buffer matrix structure than the GP37 composite, consequently, cycle-ability of the GP55 composite is superior. These phenomena are related to the GP55 composite electrode expansion ratio is lower than the GP37 composite and the pore volume of the GP55 composite is larger than that of the GP37 composite.
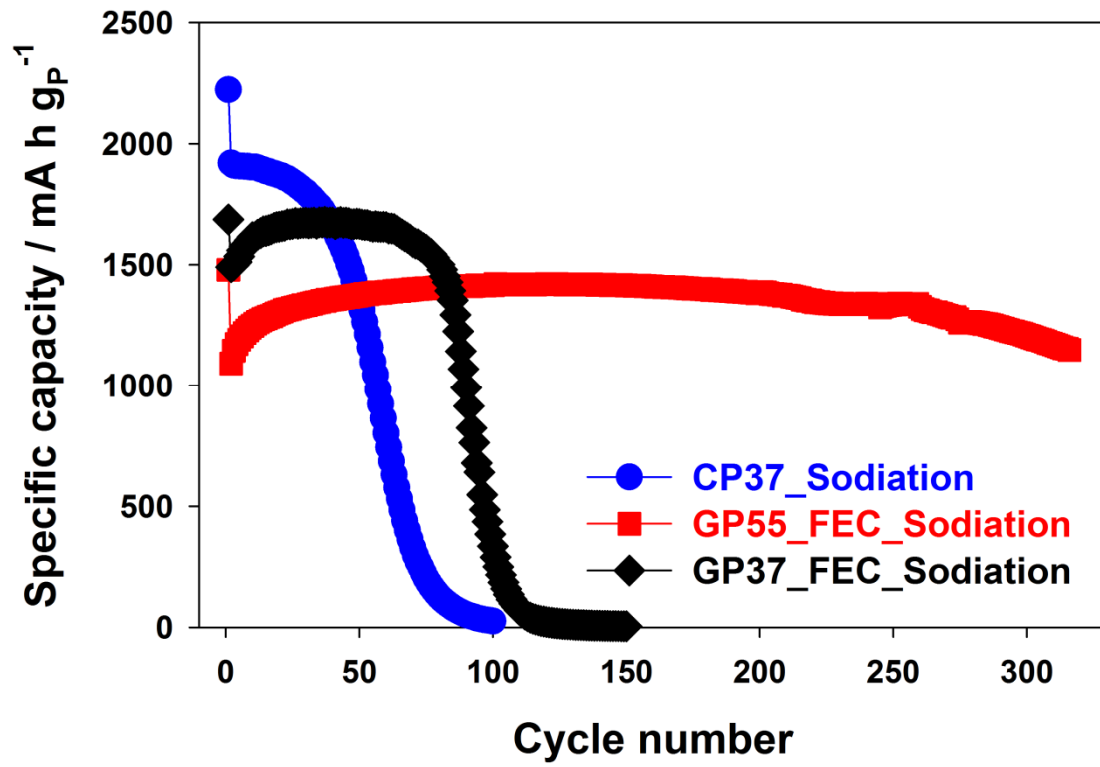
Figure 10. Comparison of cycle performances CP37, GP55, and GP37 for NIBs
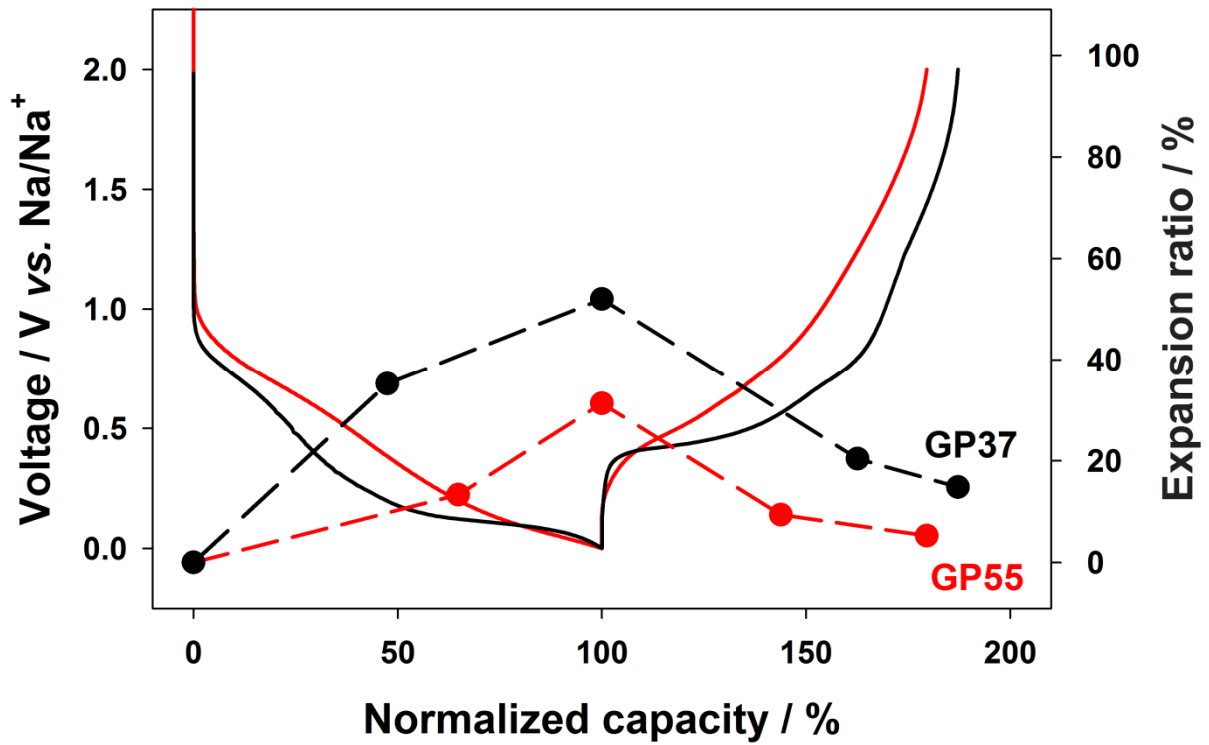
Figure 11. Voltage profiles of GP55 (red line) and GP37 (black line) and the corresponding electrode thickness change during sodiation and desodiation (red circle: GP55 , black circle: GP37)

a)
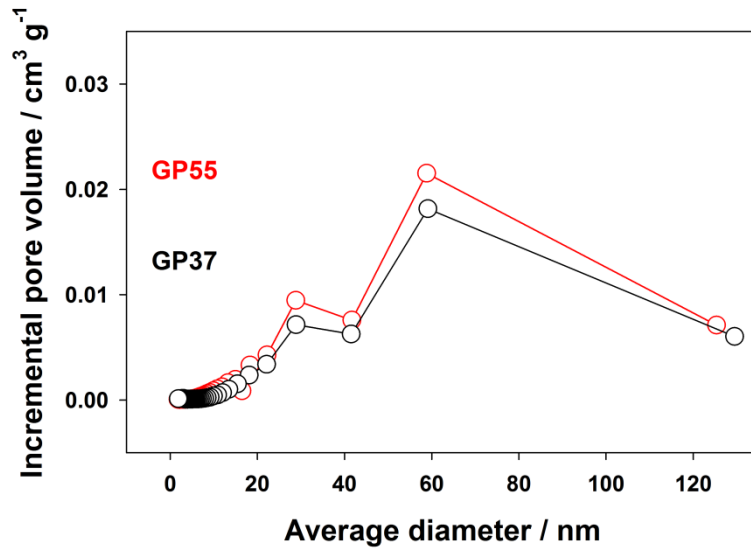
b)
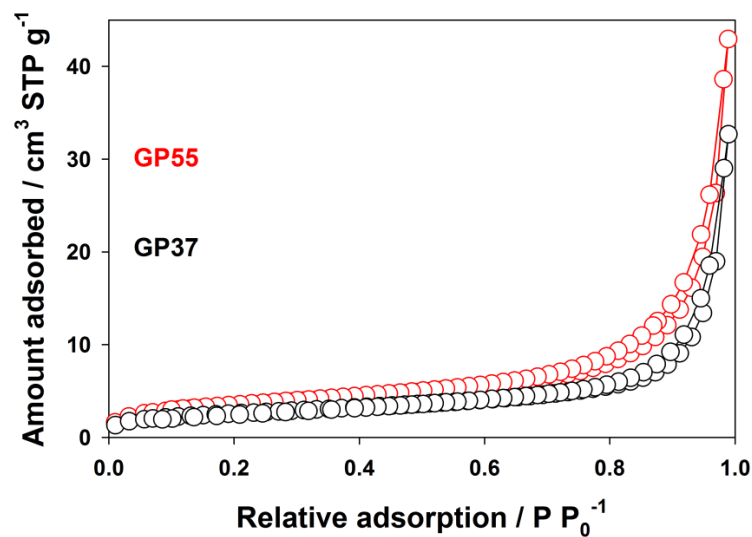
Figure 12. Physisorption analysis of GP55 and GP37: a) pore diameter, b) nitrogen adsorption/desorption isotherms

Table 2. Pore volume and surface area

	GP37	GP55
Pore Volume (cm^3/g)	0.050567	0.066432
Surface Area (m^2/g)	8.9214	11.9431

4.2 Effect of electrolyte additive FEC and failure mechanism for the composite

4.2.1 Electrochemical performances for the composite

The electrochemical performance of the GP55 composite is conducted, that is a type of half-cell with a sodium metal as a counter and reference electrode at the same time. The GP55 composite is evaluated from 2 types of electrolytes whether using fluoroethylene carbonate (FEC) as an additive (abbreviation for 'FEC') or not (abbreviation for 'FEC free'). Figure 13 shows the electrochemical performances (charging capacity) of the GP55 FEC free and the GP55 FEC electrodes between 0.0 and 2.0 V at the constant current density of 200 mA g^{-1}. In the case of 1.0 M NaClO$_4$ / EC : DEC (v : v, 1 : 1) (FEC free case), the coulombic efficiency of the 1st cycle is 73.5%, and the efficiency of the 2nd cycle is >97.3%. On the other hand, in the case of 1.0 M NaClO$_4$ / EC : DEC (v : v, 1 : 1) with 5 wt. % FEC (FEC case), the coulombic efficiency of the 1st cycle was 70%, and the efficiency of the 2nd cycle was >98% (Figure 13b). The lower 1st cycle coulombic efficiency of the FEC case is attributed to the FEC decomposition and formation of different solid electrolyte interphase (SEI) layers. But in terms of the continuous coulumbic efficiency, the FEC case can improve the coulombic efficiency than the FEC free case, because of formation stable SEI layers for anodes of the NIBs.[24,28,29,31] In the Figure 13a, both the FEC case and the FEC free case show excellent cycle performances of the GP55 composite electrodes, where the capacity fadings of the two cases are negligible over 300th cycles. In terms of the cycle-ability for the FEC free case, it performs that capacity increases up to 93rd cycle, and shows stable cycle-ability and high coulombic efficiency over 300th cycles (Figure 13). Moreover, in Figure 13, the FEC free case shows that the specific capacity is about 1459 mA h g^{-1} at the constant current density of 200 mA g^{-1}. On the other hand, the FEC case shows that the specific capacity is about 1422 mA h g^{-1} at the constant current density of 200 mA g^{-1}, and an excellent cycle performance with negligible capacity fading over 300th cycles. And it performs that capacity increases up to 121st cycle, and shows stable cycle-ability and high coulombic efficiency comparing with the FEC free case. (Figure 13) Also, differential capacity (dQ/dV) plots of the GP55 FEC free and the GP55 FEC are demonstrated in Figure 14 and 15. The GP55 FEC free case is compared and demonstrated of 1st, 5th, 50th, 93rd, 200th, and 300th cycle in Figure 14. In Figure 14a, it increases amount of the reaction and decreases polarizaion in

subsequent cycling. But in Figure 14b, it decreases amount of the reaction and increases polarization from the point of view of long cyclings. Also, the redox potential of the GP55 FEC free is ca. 0.31 V *vs*. Na/Na$^+$. The GP55 FEC case is compared and demonstrated of 1st, 5th, 61st, 121st, 210th, and 300th cycle in Figure 15. In Figure 15a, it increases amount of the reaction and decreases polarization in subsequent cycling. But in Figure 15b, it decreases amount of the reaction and increases polarization from the point of view of long cyclings in the same manner. And the redox potential of the GP55 FEC is ca. 0.30 V *vs*. Na/Na$^+$. In the 1st cycle, the FEC case undego more polarization than the FEC free case, this result causes lower 1st cycle reversible capacity for the FEC case. More polarization of the FEC case is derived from formation of different SEI layers which are based on the FEC additive. But, after 1st cycle, the FEC case has less polarizaion than the FEC free case in the activation processes (Figure 14a, 15a), and decreasing amount of the reaction and increasing amount of the polarizaion of the FEC case are less than those of the FEC free case (Figure 14b, 15b). Also, the redox potential of the FEC case is smaller than that of the FEC free case. These phenomena correspond with cycle performances (Figure 13). Additionally, although the two cases are reassembled (changing a new electrolyte and a new sodium metal) in Figure 13a, capacities of the two cases are decreased. So, we can indirectly know that active materials are degraded.

Then, the rate capabilities of the GP55 FEC free and the GP55 FEC are evaluated (Figure 16). To investigate the rate capabilities of the half cells, sodium insertion and deinsertion capacities are measured at the various constant current densities during charging and discharging processes. As shown in Figure 16, generally, the FEC case shows better rate performance than the FEC free case, and obviously showing that the FEC case delivers about 700 mA h g^{-1} even at 4 A g^{-1}, comparing with the FEC free case delivers about 83 mA h g^{-1} at 4 A g^{-1}. Therefore, the FEC additive has not only a positive effect on the cycle performance and the coulombic efficiency, but also the better rate performance of the GP55 composite. These results for the cycle performances and the rate capabilities are related to having different composition of SEI layers.

a)
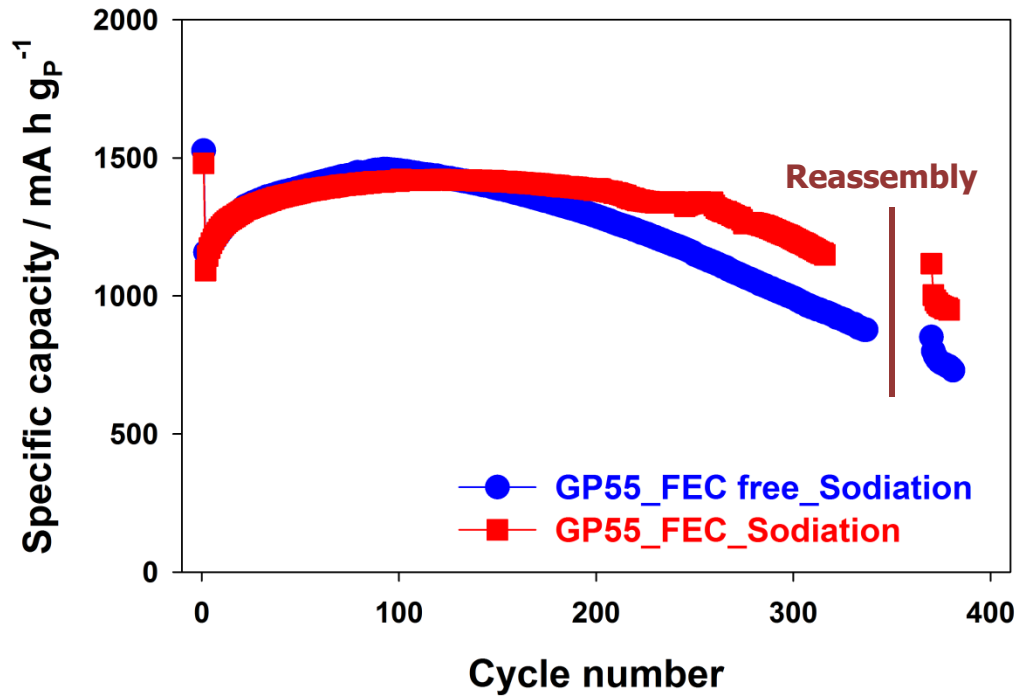
b)
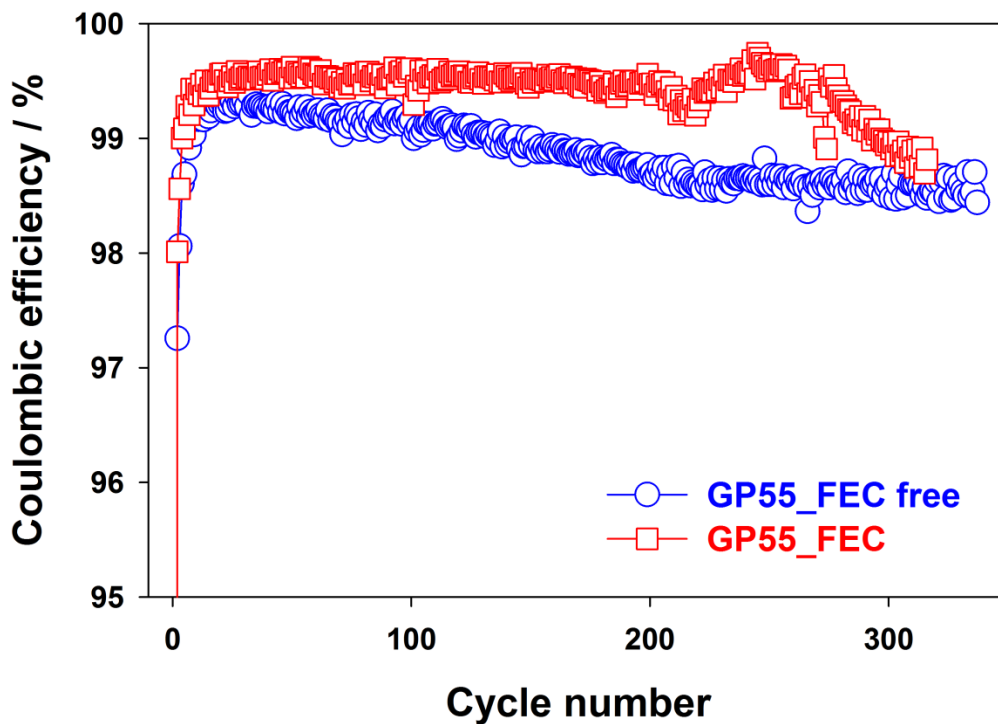
Figure 13. Comparison of cycle performances between GP55 FEC free and GP55 FEC for NIBs: a) specific capacity, b) coulombic efficiency
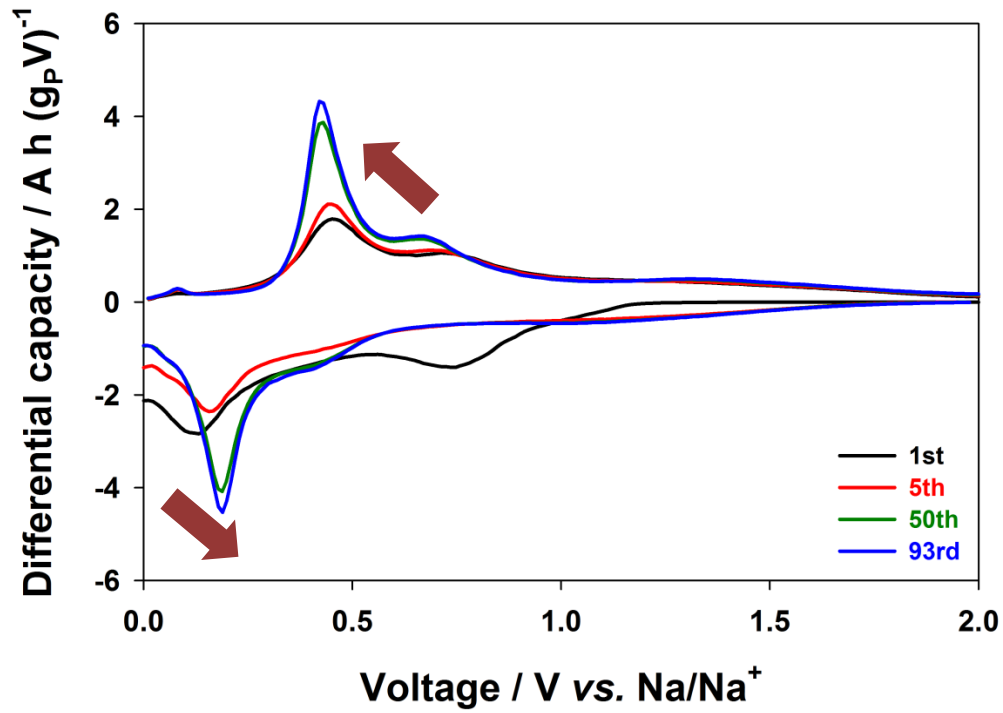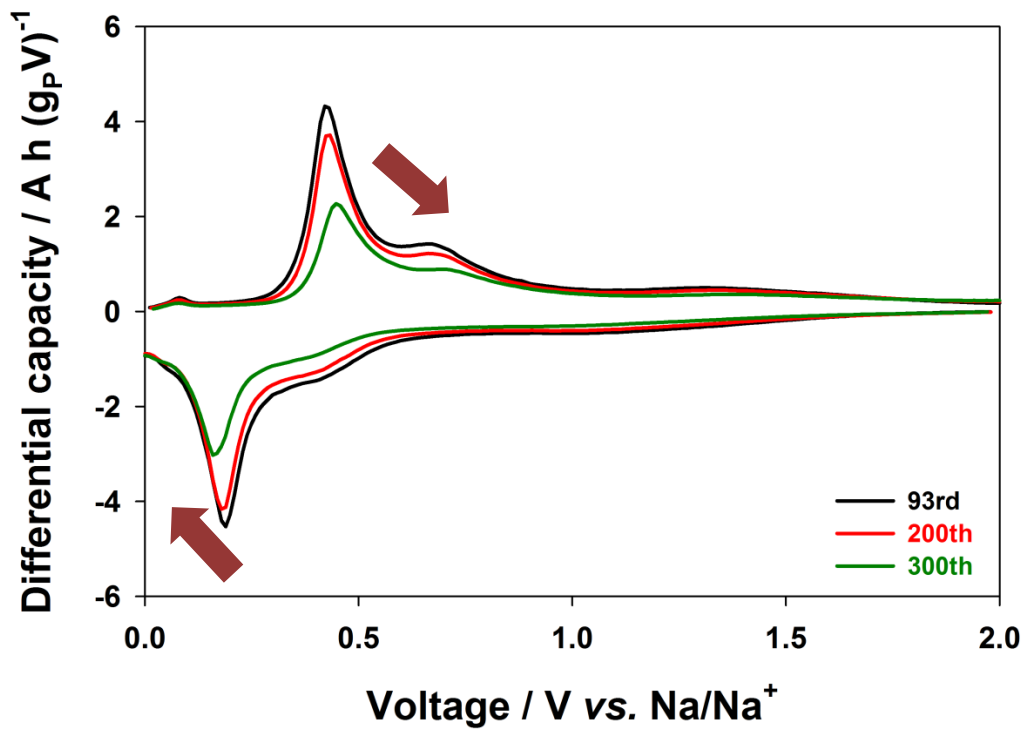
Figure 14. Differential capacity (dQ/dV) plots of GP55 FEC free: a) 1st, 5th, 50th, and 93rd cycle, b) 93rd, 200th, 300th cycle
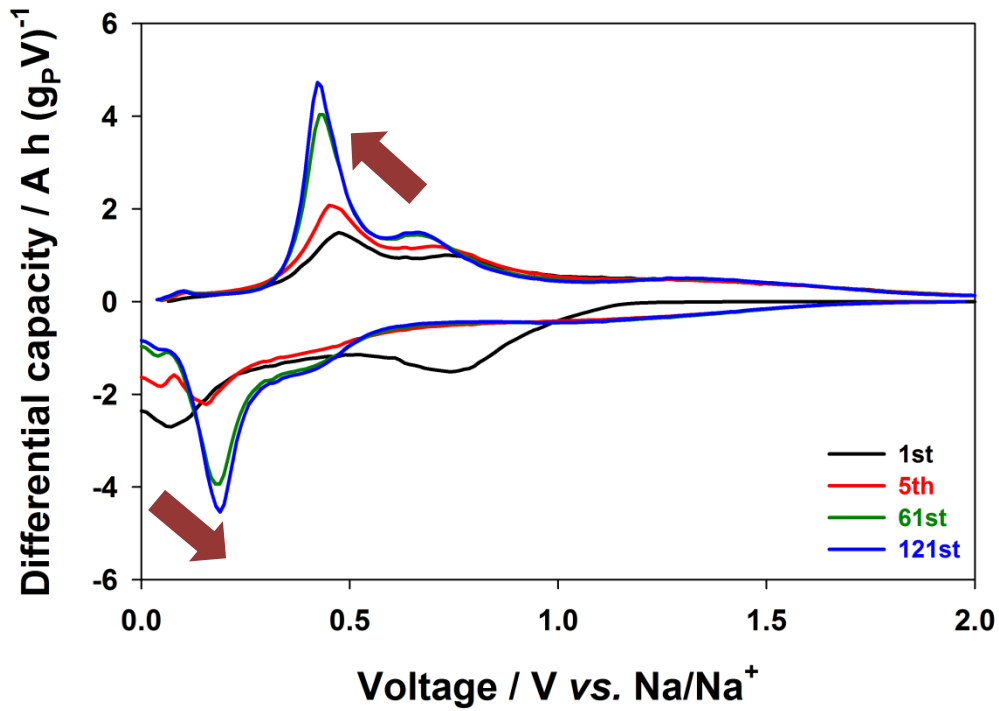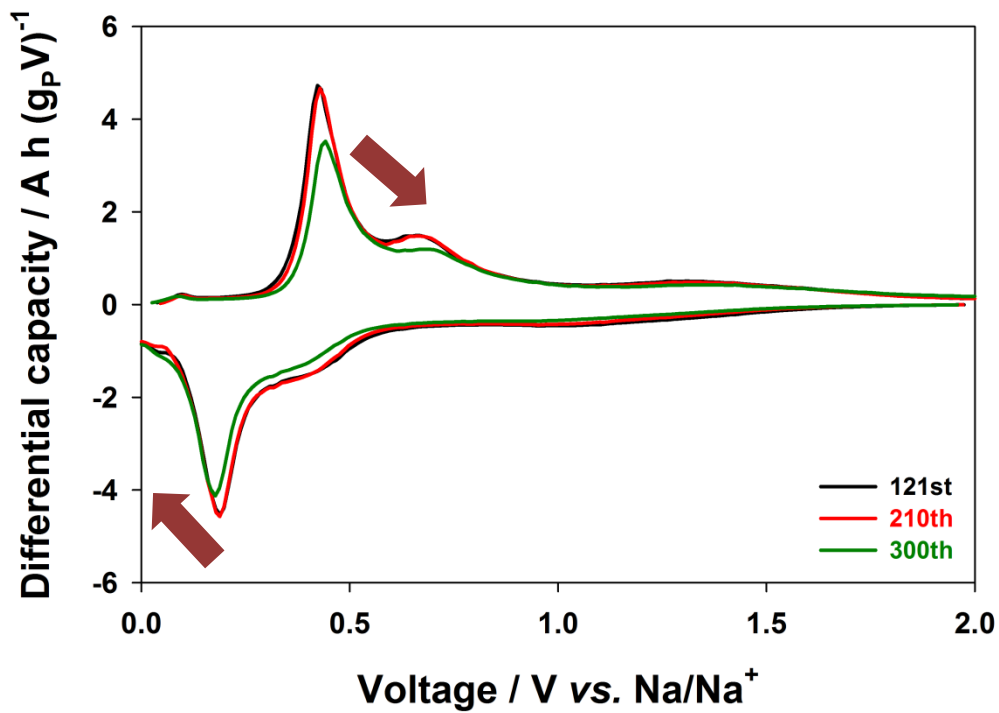
Figure 15. Differential capacity (dQ/dV) plots of GP55 FEC: a) 1st, 5th, 61st, and 121st cycle, b) 121st, 210th, 300th cycle

Figure 16. Comparison of rate capabilities between GP55 FEC free and GP55 FEC for NIBs

4.2.2 Surface analysis for the composite and the Na metal

The FEC case shows better performances than the FEC free case. In order to investigate these phenomena, we carry out analysis of the electrochemical impedance spectroscopy (EIS) as symmetric cells and analysis for the X-ray photoelectron spectroscopy (XPS).

Approaching EIS which is based on the application of symmetric cells is applied to obviously separate the activity level each of the working electrode and the counter electrode. Theref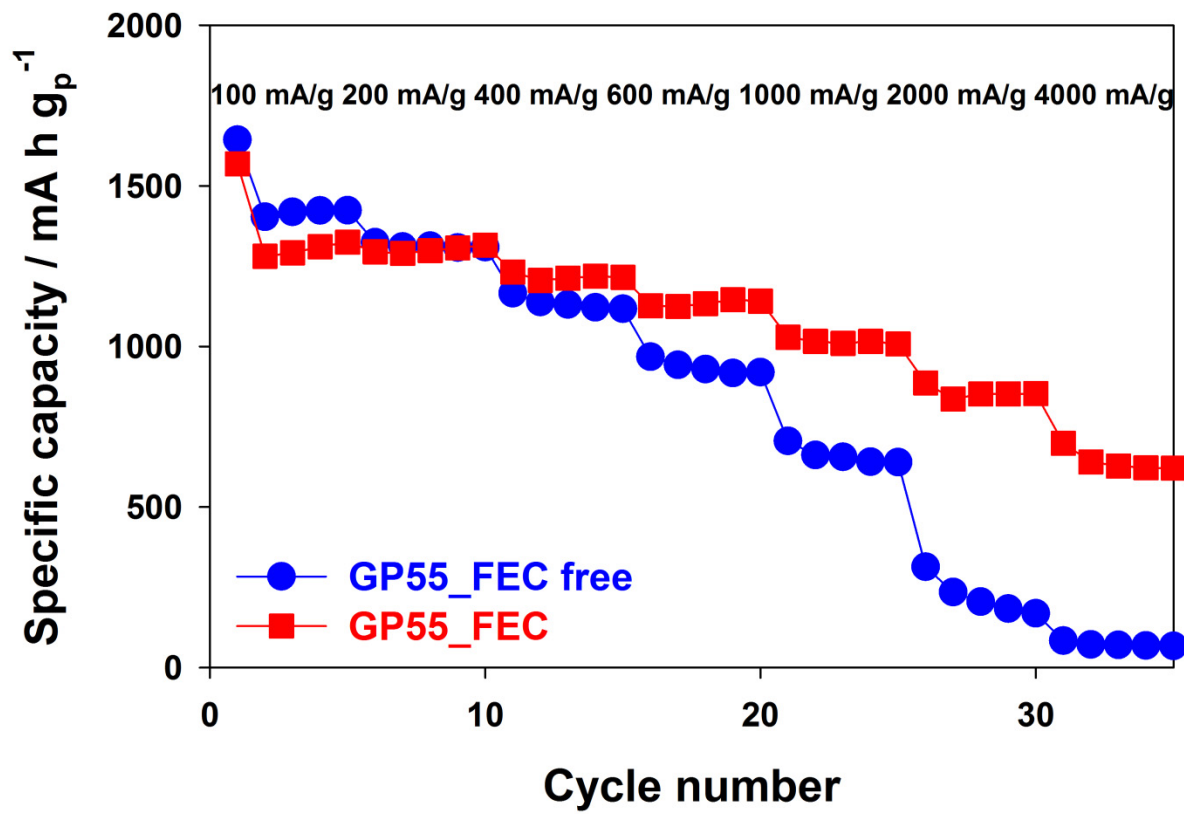ore, this symmetric cell application is able to research the working electrode and the counter electrode separately. In this research, this application allows to identify the effect of the FEC free case and the FEC case on the charge transfer resistance (R_{ct}) of the working electrode and the R_{ct} of the counter electrode. The surfaces of the working electrode and the counter electrode can be compared from the R_{ct} of each electrode. Hence, the effect of the FEC free case and the FEC case on the working electrode and the counter electrode can be identified from comparing the R_{ct} of each electrode.[44,45] In this research, the working electrode is the GP55 composite and the counter electrode (at the same time as the reference electrode) is the sodium (Na) metal. Here, EIS measurements are done; firstly cells are cycled as pre-cycles, secondly cells are charged that are state of charge 50% (SOC 50%), thirdly cells are carefully disassembled in a glove box to retrieve their working electrodes and sodium metal electrodes, fourthly cells are reassembled like the symmetric cells (the working electrode-the working electrode, the counter electrode-the counter electrode), and then measure the EIS. From the results of the EIS, measured resistance is in inverse proportion to weight of active material (the working electrode). Weight of the working electrodes are almost same, but to express clearly, multiply measured resistance and used active material weight together, and the value is represented in Figure 17. Also, in the case of the sodium metal electrodes, weight and surface area of the sodium metal electrodes are almost same, multiply measured resistance and used sodium metal surface area together, and the value is represented in Figure 18.[46] In Figure 17, in the symmetric cells of the working electrodes, they show that the non-additive case and the FEC additive case have different effects on the R_{ct} of the GP55 composite electrodes. The FEC case leads to lower R_{ct} than the FEC free case. This phenomenon implies that the FEC case makes the different composition of surface from the FEC free case does. Likewise, in Figure 18, in the symmetric cells of the counter electrodes, they also show that the FEC free case and the FEC case have different effects on

the R_{ct} of the sodium metal electrodes. The FEC additive case leads to higher R_{ct} on the sodium metal electrode than the FEC additive case. This phenomenon is expected that different R_{ct} comes from different constituents of surface and original characteristics for decomposition of FEC additive. From the EIS analysis based on symmetric cells, effects of the FEC additive are different at the working electrode and the counter electrode (lower R_{ct} on the working electrode, but higher R_{ct} on the counter electrode). But, in the half cell (not symmetric cell, working electrode-counter electrode), the FEC additive case cause lower R_{ct} than the non-additive case does. It is based on Figure 14, Figure 15, and published previous paper.[22,46] Therefore, we can know that influence on the working electrode (the GP55 composite) is greater than that on the counter electrode (the sodium metal).

And, analysis of XPS is done to identify the chemical compositions of the surfaces on the electrodes. Elements (C 1s, Cl 2p, Na 1s, O 1s, F1s, and P 2p) are analyzed by XPS, also they are reported previous other papers.[22,28,29,31] Firstly cells are cycled as pre-cycles, secondly cells are carefully disassembled in a glove box to retrieve their electrodes and metals, and then they are analyzed by XPS. In the Figure 19, they show that F 1s spectra for the FEC free case (Figure 19a, 19c) and the FEC additive case (Figure 19b, 19d) on the electrode and the Na metal. To clearly analyze, the etching processes are done on the both surfaces and Figure 19 are appeared by etching for 60 seconds. In FEC free case, there are not any peaks for F 1s on the both surfaces. (Figure 19a, 19c) On the other hand, in the FEC case, there is one pronounced F 1s peak which is related to the NaF-like compound[22] on the both surfaces. (Figure 19b, 19d) These figures demonstrate that FEC component is decomposed and the decomposed FEC component turns to the NaF-like compound one of the SEI layers constituents.

Additionally, P 2p XPS spectra are conducted on the GP55 composite electrodes by etching depth profiling analysis. Totally, 4 kinds of sample (the red phosphorus powder, the GP55 composite powder, the FEC free electrode, and the FEC electrode) are analyzed. In the P 2p XPS spectra, there are two evident peaks which are related to the red phosphorus and the P-O bonding compound.[29] In case of the red phosphorus powder (Figure 20a), seeing the etching depth profile, only surface of the active material (the red phosphorus) is oxidized. On the other hand, in case of the GP55 composite powder (Figure 20b), seeing the etching depth profile, oxidation of the active material can be seen in depth (by ratio of P-O to Red P). This cause of a phenomenon is assumed that during mechanochemical ball milling synthesis, very

small amount of water and oxygen element included gases (oxygen, carbon dioxide, and so on) can oxidize the phosphorus in depth and the resulting composite powder is oxidized by exposing to air moisture as state of the phosphorus is acceptable oxygen element.[42] Therefore, the GP composite powder has an oxidized phosphorus constituent to some degree in depth. Then, the GP55 FEC free electrode and the GP55 FEC electrode are analyzed. In Figure 21, comparing between the FEC free case (Figure 21a) and the FEC case (Figure 21b), the FEC free case has the higher value (ratio of P-O to Red P) than the FEC case. This point indicates that the amount of oxidized active material in the FEC case is more than that in the FEC free case. Oxidizing active material is caused by decomposition of electrolyte. Also, the Figure 21 is expressed as the graph in the Figure 22.

Moreover, O 1s spectra are showed for the electrodes (Figure 23a, 23c) and the Na metals (Figure 23b, 23d) both the FEC free case and the FEC case. To clearly analyze, the etching processes are done on the both surfaces and Figure 23 are appeared by etching for 60 seconds. In the O 1s XPS spectra, there are four peaks which are related to the C=O bonding compounds,[47] the C-O-C bonding compounds,[48] and the two Na KLL Auger peaks.[49] On the electrode, they have different SEI composition between the FEC free case and the FEC case from the point of O 1s XPS spectra. But on the Na metal, they have similar SEI composition between both cases from the point of O 1s XPS spectra. In Figure 23a and 23c, there are many C=O bonding compound and C-O-C bonding compound in the FEC free case. But in the FEC case, it has less C-O-C bonding compound. Hence, different SEI compound are formed on the electrodes from the point of O 1s XPS spectra. In Figure 23b and 23d, they don't have big differences between both cases, and similar SEI compound are formed on the Na metals from the point of O 1s XPS spectra.

Putting them all together (EIS and XPS), on the working electrode (the GP55 composite), R_{ct} of the non-additive case is greater than that of the FEC additive case, because of the different constituents on the surface. Active material is oxidized by decomposition of the electrolyte. Oxidized active material forms P-O bonding, that compound act as increasing R_{ct} element. Therefore, reasons of degrading active material (the GP55 composite) are that not only severe volume expansion and shrinkage which cause contact loss, but also the oxidized active material causes contact loss. The amount of P-O bonding element is larger in the FEC free case. On the other hand, in the FEC case, the FEC are reduced and decomposed in the 1st cycle, and forms NaF-like compound. This NaF-like compound can inhibit oxidation of the

active material and these surface compositions reduce R_{ct} on the working electrode and make excellent cycle-ability, coulombic efficiency, and rate capability comparing with the FEC free case. These processes are described as a schematic diagram in the Figure 24.

Whereas on the Na metals, R_{ct} of the FEC case is greater than that of the FEC free case. The result is different from the working electrodes. Because the constituents of the SEI layers are similar except for forming NaF compound whether or not. NaF compound is like as LiF compound. LiF compound is known for having bad ionic and electronic conductivity.[50-52] Hence, R_{ct} of the FEC case is larger. These processes are described as a schematic diagram in the Figure 25.
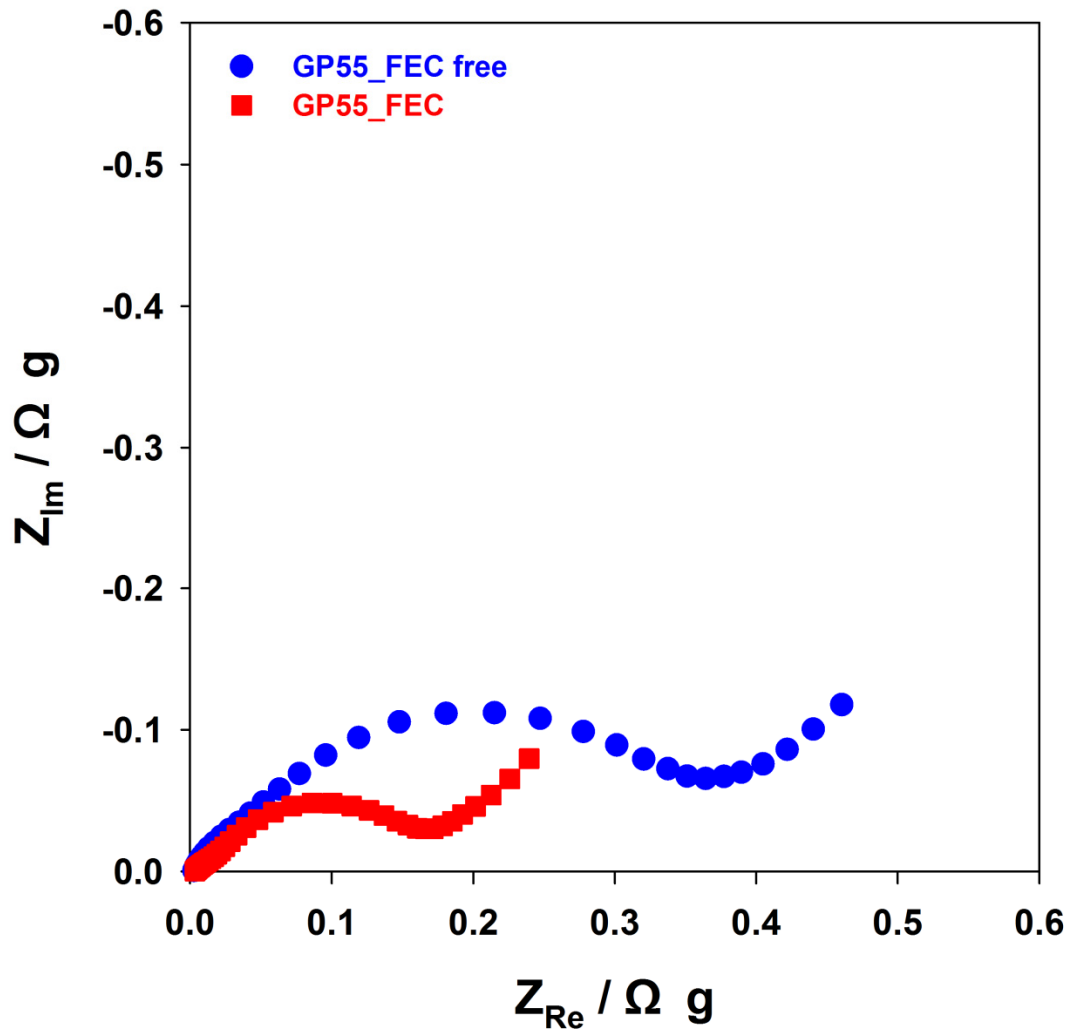
Figure 17. Measuring symmetric cell impedance of electrodes and comparison between GP55 FEC free and GP55 FEC
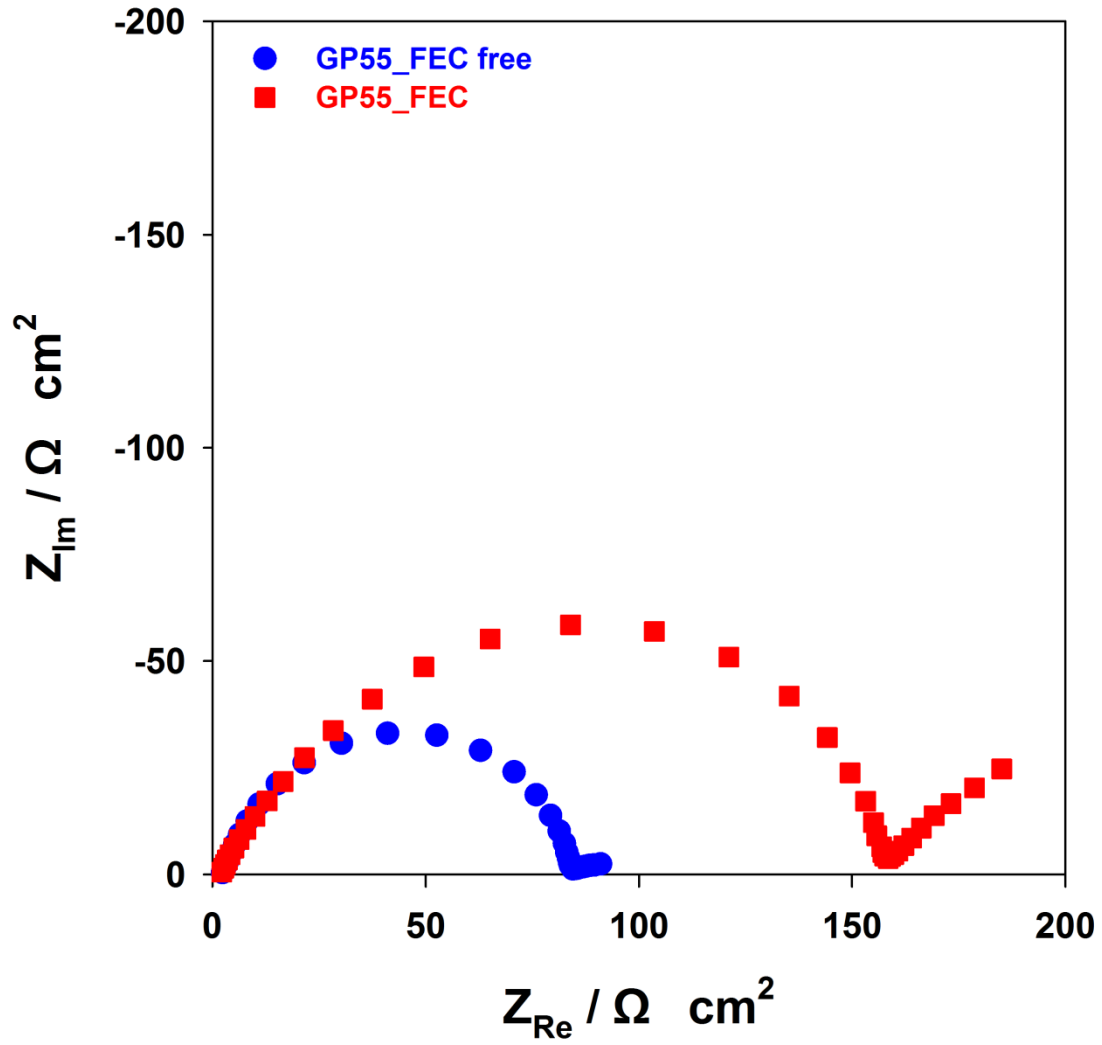
Figure 18. Measuring symmetric cell impedance of Na metals and comparison between GP55 FEC free and GP55 FEC
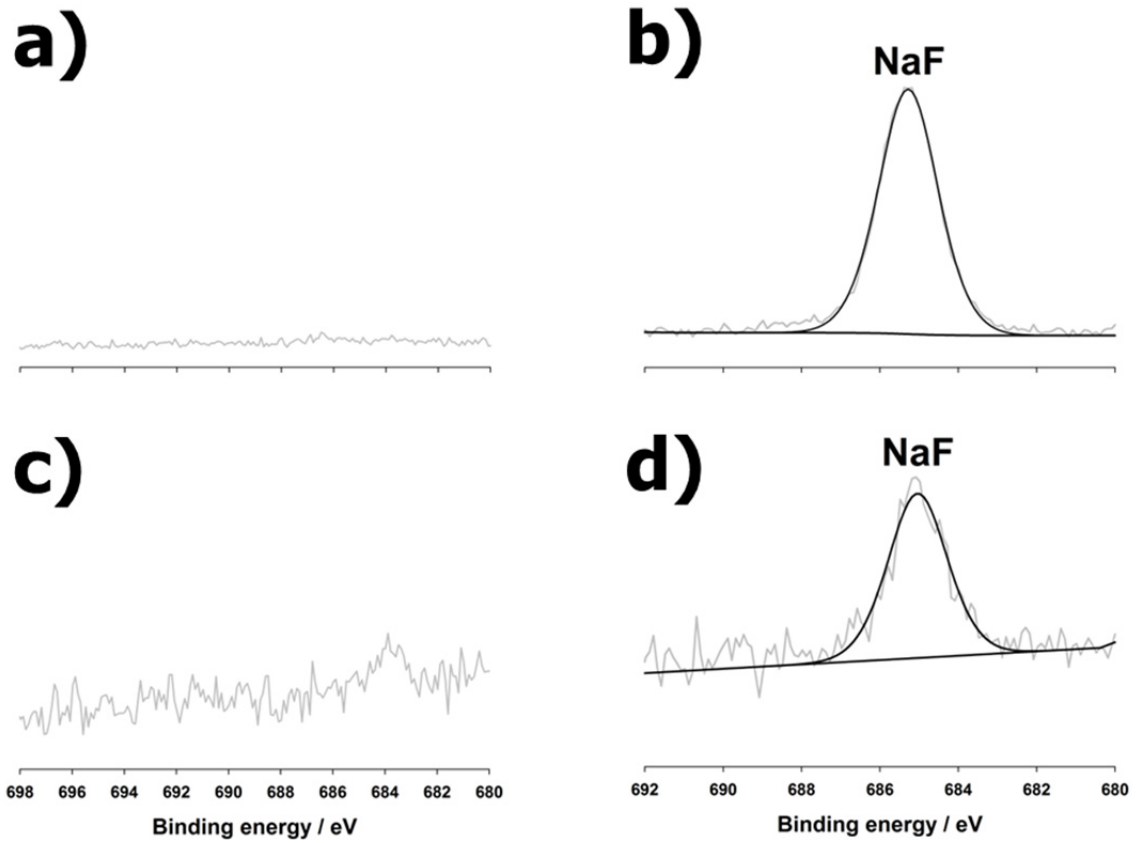
Figure 19. F 1s XPS spectra obtained from: a) Electrode - FEC free, b) Electrode - FEC c) Na metal - FEC free, d) Na metal - FEC
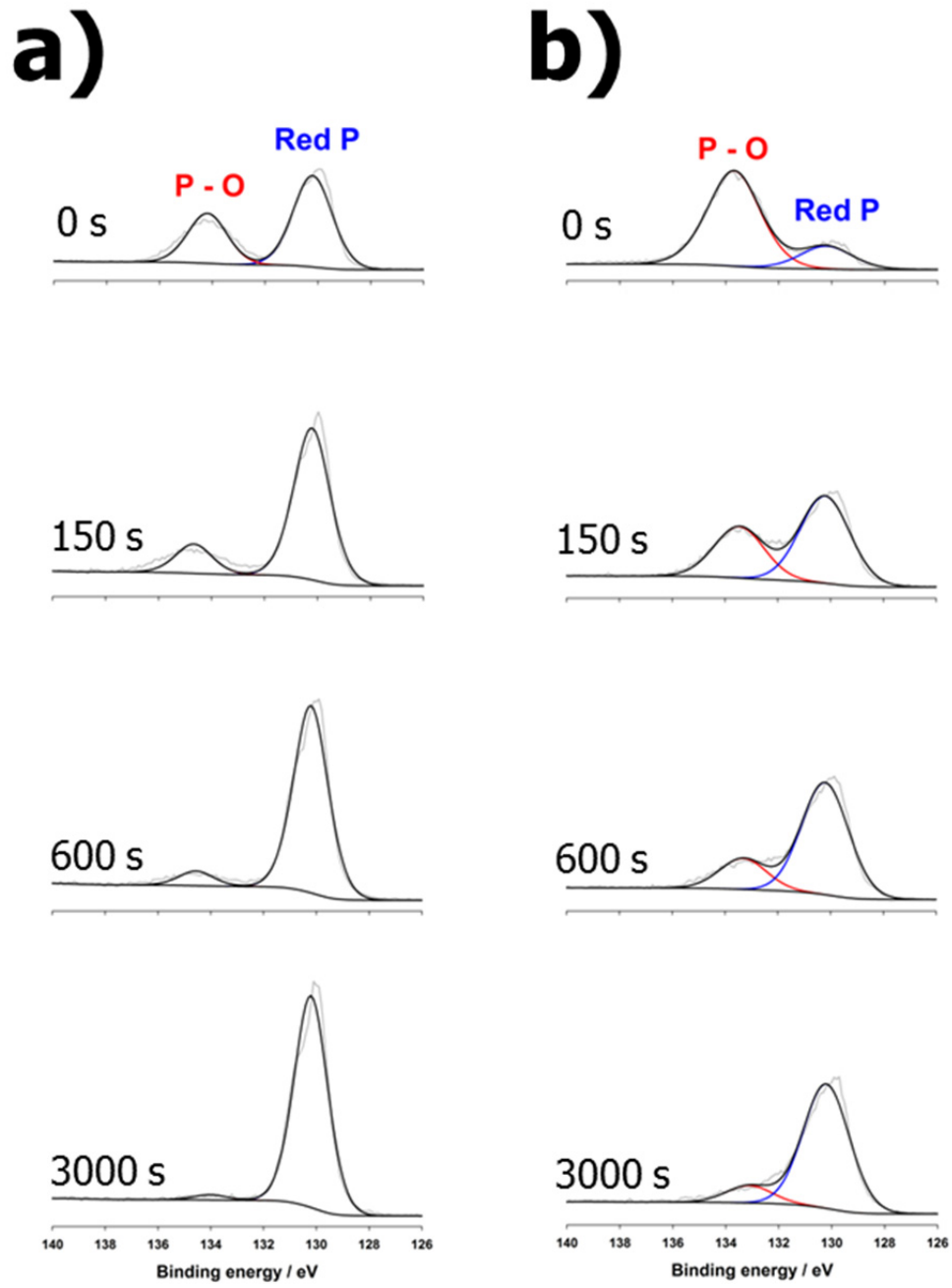
Figure 20. P 2p XPS spectra through depth profile analysis: a) Red P powder, b) GP55 powder
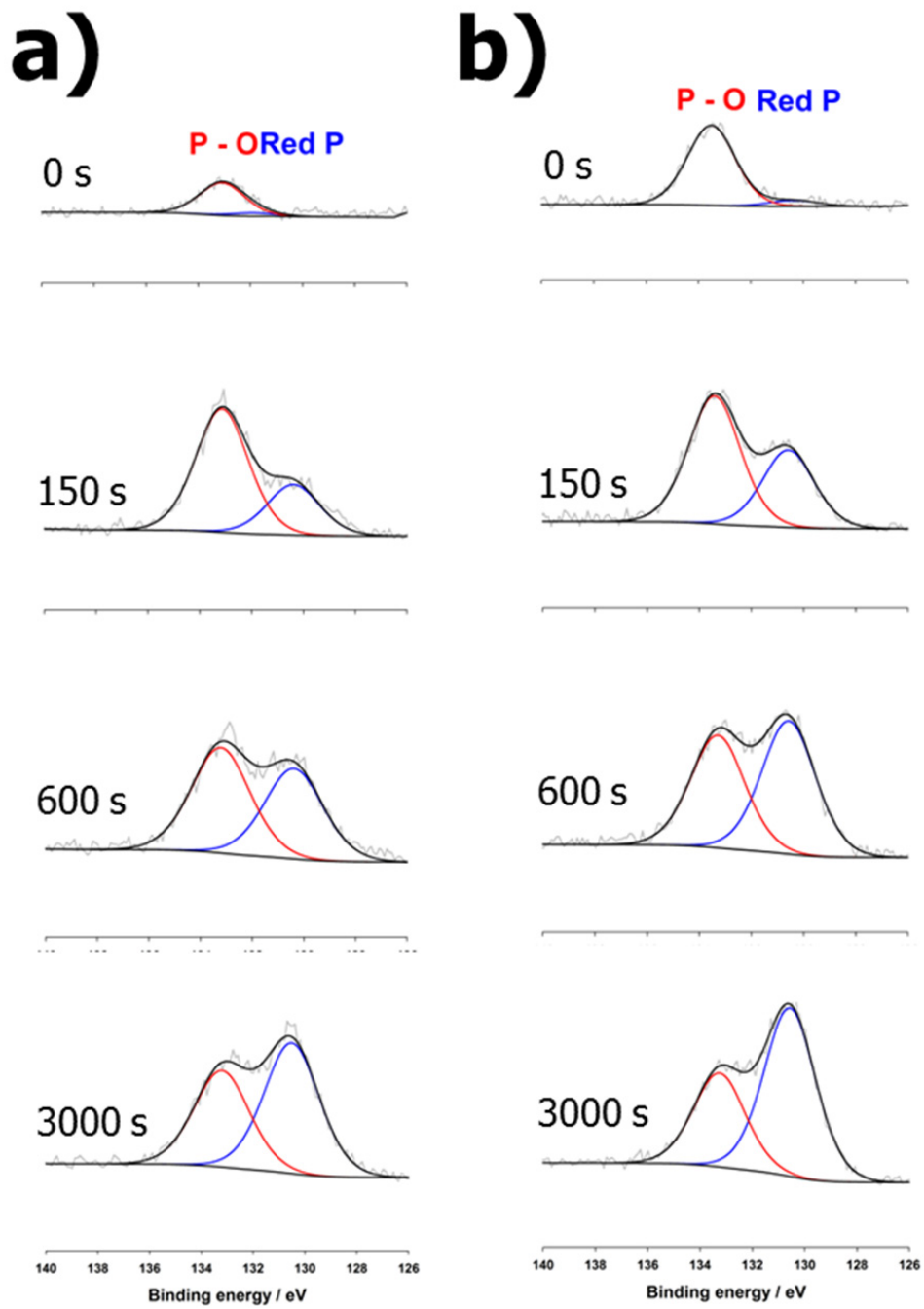
Figure 21. P 2p XPS spectra through depth profile analysis: a) GP55 FEC free electrode, b) GP55 FEC electrode
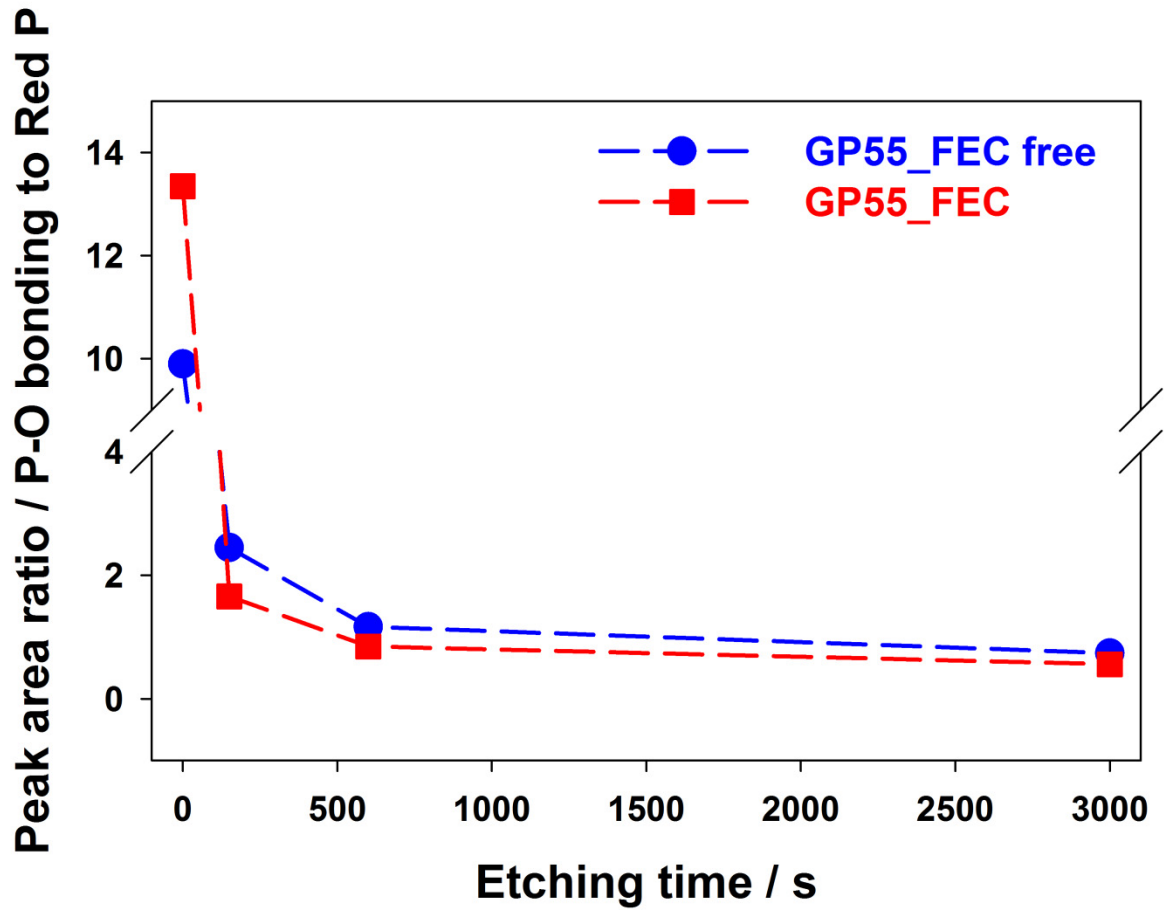
Figure 22. P 2p XPS spectra ratio of P-O bonding to Red P through depth profile analysis: comparison between GP55 FEC free electrode and GP55 FEC electrode
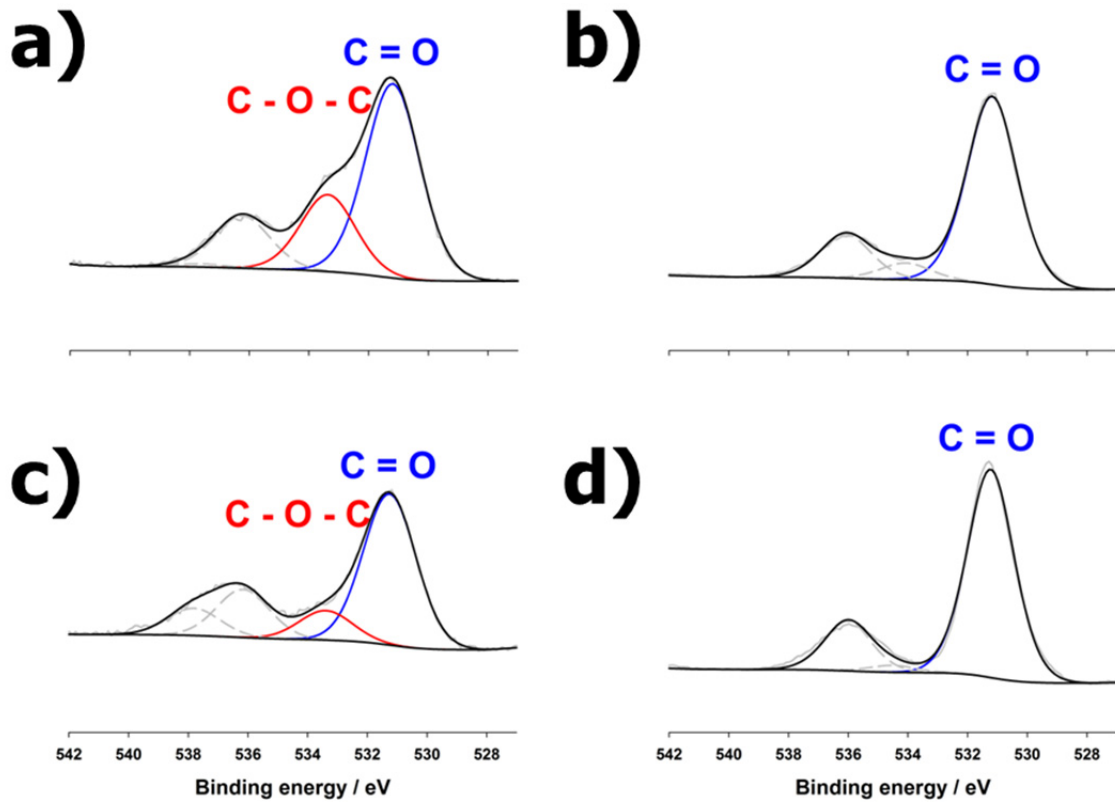
Figure 23. O 1s XPS spectra obtained from: a) Electrode – FEC free, b) Na metal – FEC free, c) Electrode – FEC, d) Na metal – FEC
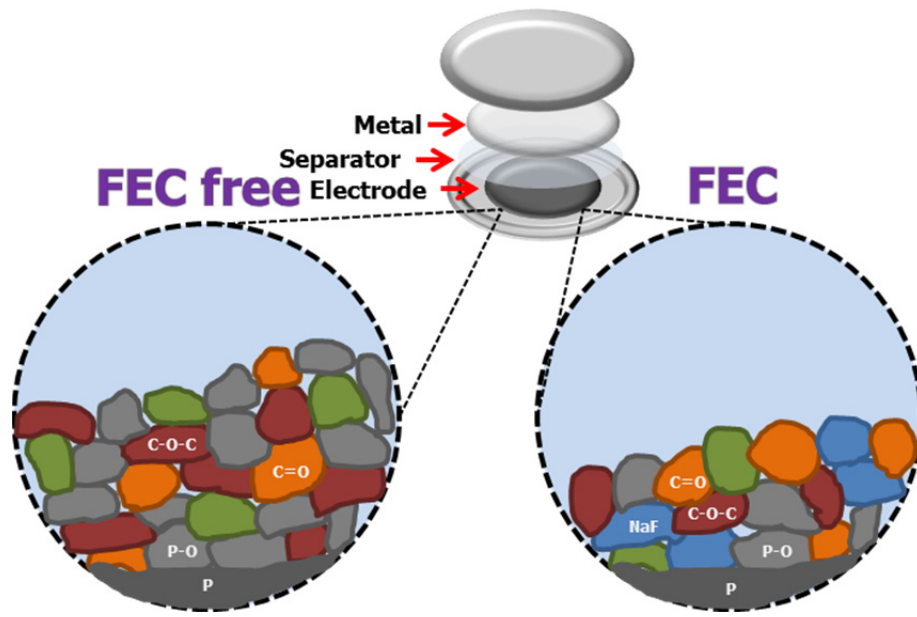
Figure 24. Schematic diagram of electrode surfaces: comparison between FEC free and FEC
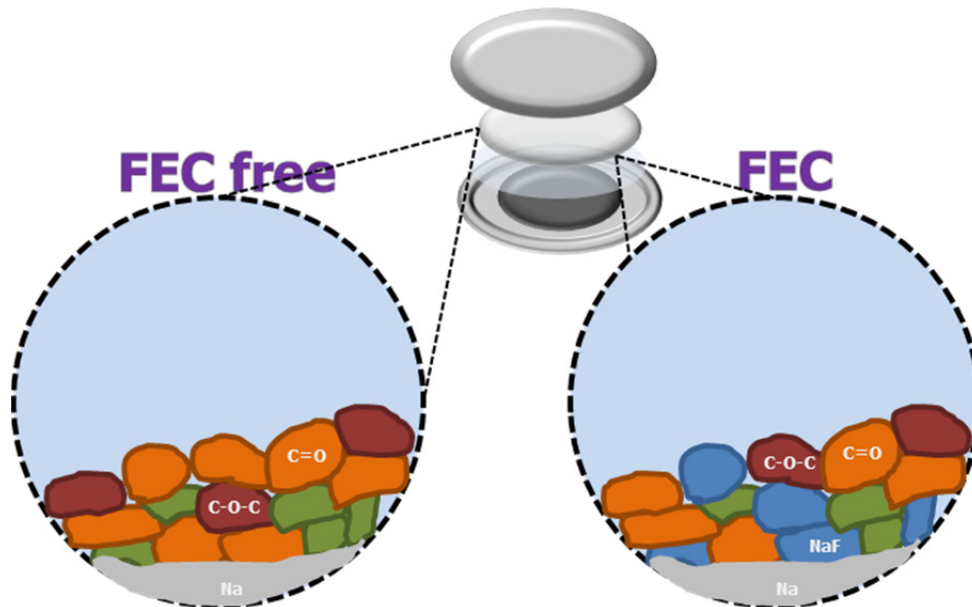
Figure 25. Schematic diagram of metal surfaces: comparison between FEC free and FEC

Ⅴ. Conclusion

In conclusion, the phosphorus/graphite composites (the GP55 and the GP37 composite) are obtained by simple mechanochemical ball milling. Electrochemical performances of the two composites as an anode material for NIBs are better and stable comparing with previous reported papers. Among them, the GP37 composite has more initial reversible capacities than the GP55 composite, because of different ionic conductivity. And the GP55 composite has more stable cycle-ability than the GP37 composite, because of the different amount of amorphization and pore volume. That causes a smaller changing for electrode thickness of the GP55 composite. Also because graphite surface coverage of the GP55 composite is wider than that of the GP37 composite, surface oxidation of the active material (the red phosphorus) in the GP55 composite is less than that in the GP37 composite. It also affects the cycle-ability.

Also, via the FEC free case and the FEC case on the GP55 composite, the FEC case shows better cycle performances. The FEC additive inhibits the oxidation of the active material (the red phosphorus), resulting in excellent cycle performances of the composite. These phenomena are analyzed by EIS on symmetric cells and XPS analysis. As a result, there are two representative causes of the degradation. One is that the active material (the red phosphorus) has severe volume expansion and shrinkage which cause contact loss, and by the XPS analysis, the other is that the oxidized active material causes contact loss. Also, the results indicate that effects between the working electrodes and the counter electrodes are different. Therefore, we should consider differences between half-cell type and full-cell type.

Finally, LIBs based technologies and researches have been developed for decades. Understanding and applying LIBs based them, NIBs based technologies and researches will be progress fast and efficiently. Not only similarities of LIBs cause accelerating the development of NIBs parts, but also the growth of NIBs technologies and researches may give directions to absolutely improved energy conversion and storage systems as the breakthrough. Therefore, we need to research more and more about active materials for electrodes, electrolytes with additives, and especially electrode/electrolyte interphase. These researches will advance practical and commercialized NIBs.

References

1   Dunn, B., Kamath, H. & Tarascon, J.-M. Electrical Energy Storage for the Grid: A Battery of Choices. *Science* **2011**, 334,928-935.

2   Ellis, B. L., Lee, K. T. & Nazar, L. F. Positive Electrode Materials for Li-Ion and Li-Batteries†. *Chem. Mater.* **2010**, 22,691-714.

3   Choi, N. S., Chen, Z., Freunberger, S. A., Ji, X., Sun, Y. K., Amine, K., Yushin, G., Nazar, L. F., Cho, J. & Bruce, P. G. Challenges Facing Lithium Batteries and Electrical Double-Layer Capacitors. *Angew. Chem., Int. Ed.* **2012**, 51,9994-10024.

4   Lee, K. T. & Cho, J. Roles of nanosize in lithium reactive nanomaterials for lithium ion batteries. *Nano Today* **2011**, 6,28-41.

5   Goodenough, J. B. & Kim, Y. Challenges for rechargeable Li batteries. *Chem. Mater.* **2009**, 22,587-603.

6   Hong, S. Y., Kim, Y., Park, Y., Choi, A., Choi, N.-S. & Lee, K. T. Charge carriers in rechargeable batteries: Na ions vs. Li ions. *Energy Environ. Sci.* **2013**, 6,2067-2081.

7   Dahbi, M., Yabuuchi, N., Kubota, K., Tokiwa, K. & Komaba, S. Negative electrodes for Na-ion batteries. *Phys. Chem. Chem. Phys.* **2014**, 16,15007-15028.

8   Kim, Y., Ha, K.-H., Oh, S. M. & Lee, K. T. High-Capacity Anode Materials for Sodium-Ion Batteries. *Chem. Eur. J.* **2014**, 20,11980-11992.

9   Peled, E. The Electrochemical Behavior of Alkali and Alkaline Earth Metals in Nonaqueous Battery Systems—The Solid Electrolyte Interphase Model. *J. Electrochem. Soc.* **1979**, 126,2047-2051.

10   Kim, Y., Park, Y., Choi, A., Choi, N.-S., Kim, J., Lee, J., Ryu, J. H., Oh, S. M. & Lee, K. T. An Amorphous Red Phosphorus/Carbon Composite as a Promising Anode Material for Sodium Ion Batteries. *Adv. Mater.* **2013**, 25,3045-3049.

11   Yabuuchi, N., Kubota, K., Dahbi, M. & Komaba, S. Research Development on Sodium-Ion Batteries. *Chem. Rev.* **2014**, 114,11636-11682.

12   Chevrier, V. L. & Ceder, G. Challenges for Na-ion Negative Electrodes. *J. Electrochem. Soc.* **2011**, 158,A1011-A1014.

13   Ellis, L. D., Hatchard, T. D. & Obrovac, M. N. Reversible Insertion of Sodium in Tin. *J. Electrochem. Soc.* **2012**, 159,A1801-A1805.

14   Komaba, S., Matsuura, Y., Ishikawa, T., Yabuuchi, N., Murata, W. & Kuze, S. Redox reaction of Sn-polyacrylate electrodes in aprotic Na cell. *Electrochem. Commun.* **2012**, 21,65-68.

15   Xu, Y., Zhu, Y., Liu, Y. & Wang, C. Electrochemical Performance of Porous Carbon/Tin Composite Anodes for Sodium-Ion and Lithium-Ion Batteries. *Adv. Energy Mater.* **2013**,

3,128-133.

16   Darwiche, A., Marino, C., Sougrati, M. T., Fraisse, B., Stievano, L. & Monconduit, L. Better Cycling Performances of Bulk Sb in Na-Ion Batteries Compared to Li-Ion Systems: An Unexpected Electrochemical Mechanism. *J. Am. Chem. Soc.* **2012**, 134,20805-20811.

17   Baggetto, L., Ganesh, P., Sun, C.-N., Meisner, R. A., Zawodzinski, T. A. & Veith, G. M. Intrinsic thermodynamic and kinetic properties of Sb electrodes for Li-ion and Na-ion batteries: experiment and theory. *J. Mater. Chem. A* **2013**, 1,7985-7994.

18   Qian, J., Chen, Y., Wu, L., Cao, Y., Ai, X. & Yang, H. High capacity Na-storage and superior cyclability of nanocomposite Sb/C anode for Na-ion batteries. *Chem. Commun.* **2012**, 48,7070-7072.

19   Qian, J., Wu, X., Cao, Y., Ai, X. & Yang, H. High Capacity and Rate Capability of Amorphous Phosphorus for Sodium Ion Batteries. *Angew. Chem.* **2013**, 125,4731-4734.

20   Fullenwarth, J., Darwiche, A., Soares, A., Donnadieu, B. & Monconduit, L. NiP3: a promising negative electrode for Li- and Na-ion batteries. *J. Mater. Chem. A* **2014**, 2,2050-2059.

21   Kim, Y., Kim, Y., Park, Y., Jo, Y. N., Kim, Y.-J., Choi, N.-S. & Lee, K. T. SnSe alloy as a promising anode material for Na-ion batteries. *Chem. Commun.* **2015**, 51,50-53.

22   Ji, L., Gu, M., Shao, Y., Li, X., Engelhard, M. H., Arey, B. W., Wang, W., Nie, Z., Xiao, J., Wang, C., Zhang, J.-G. & Liu, J. Controlling SEI Formation on SnSb-Porous Carbon Nanofibers for Improved Na Ion Storage. *Adv. Mater.* **2014**, 26,2901-2908.

23   Darwiche, A., Sougrati, M. T., Fraisse, B., Stievano, L. & Monconduit, L. Facile synthesis and long cycle life of SnSb as negative electrode material for Na-ion batteries. *Electrochem. Commun.* **2013**, 32,18-21.

24   Kim, Y., Kim, Y., Choi, A., Woo, S., Mok, D., Choi, N.-S., Jung, Y. S., Ryu, J. H., Oh, S. M. & Lee, K. T. Tin Phosphide as a Promising Anode Material for Na-Ion Batteries. *Adv. Mater.* **2014**, 26,4139-4144.

25   Farbod, B., Cui, K., Kalisvaart, W. P., Kupsta, M., Zahiri, B., Kohandehghan, A., Lotfabad, E. M., Li, Z., Luber, E. J. & Mitlin, D. Anodes for Sodium Ion Batteries Based on Tin–Germanium–Antimony Alloys. *ACS Nano* **2014**, 8,4415-4429.

26   Cabana, J., Monconduit, L., Larcher, D. & Palacín, M. R. Beyond Intercalation-Based Li-Ion Batteries: The State of the Art and Challenges of Electrode Materials Reacting Through Conversion Reactions. *Adv. Mater.* **2010**, 22,E170-E192.

27   Poizot, P., Laruelle, S., Grugeon, S., Dupont, L. & Tarascon, J. M. Nano-sized transition-metal oxides as negative-electrode materials for lithium-ion batteries. *Nature* **2000**, 407,496-499.

28 Komaba, S., Murata, W., Ishikawa, T., Yabuuchi, N., Ozeki, T., Nakayama, T., Ogata, A., Gotoh, K. & Fujiwara, K. Electrochemical Na Insertion and Solid Electrolyte Interphase for Hard-Carbon Electrodes and Application to Na-Ion Batteries. *Adv. Funct. Mater.* **2011**, 21,3859-3867.

29 Yabuuchi, N., Matsuura, Y., Ishikawa, T., Kuze, S., Son, J.-Y., Cui, Y.-T., Oji, H. & Komaba, S. Phosphorus Electrodes in Sodium Cells: Small Volume Expansion by Sodiation and the Surface-Stabilization Mechanism in Aprotic Solvent. *ChemElectroChem* **2014**, 1,580-589.

30 Jang, J. Y., Kim, H., Lee, Y., Lee, K. T., Kang, K. & Choi, N.-S. Cyclic carbonate based-electrolytes enhancing the electrochemical performance of Na4Fe3(PO4)2(P2O7) cathodes for sodium-ion batteries. *Electrochem. Commun.* **2014**, 44,74-77.

31 Komaba, S., Ishikawa, T., Yabuuchi, N., Murata, W., Ito, A. & Ohsawa, Y. Fluorinated Ethylene Carbonate as Electrolyte Additive for Rechargeable Na Batteries. *ACS Appl. Mater. Interfaces* **2011**, 3,4165-4168.

32 Moshkovich, M., Gofer, Y. & Aurbach, D. Investigation of the Electrochemical Windows of Aprotic Alkali Metal (Li, Na, K) Salt Solutions. *J. Electrochem. Soc.* **2001**, 148,E155-E167.

33 Delmas, C., Braconnier, J.-J., Fouassier, C. & Hagenmuller, P. Electrochemical intercalation of sodium in NaxCoO2 bronzes. *Solid State Ionics* **1981**, 3–4,165-169.

34 Komaba, S., Takei, C., Nakayama, T., Ogata, A. & Yabuuchi, N. Electrochemical intercalation activity of layered NaCrO2 vs. LiCrO2. *Electrochem. Commun.* **2010**, 12,355-358.

35 Vassilaras, P., Ma, X., Li, X. & Ceder, G. Electrochemical Properties of Monoclinic NaNiO2. *J. Electrochem. Soc.* **2013**, 160,A207-A211.

36 de Picciotto, L. A., Thackeray, M. M., David, W. I. F., Bruce, P. G. & Goodenough, J. B. Structural characterization of delithiated LiVO2. *Mater. Res. Bull.* **1984**, 19,1497-1506.

37 Yu, H., Guo, S., Zhu, Y., Ishida, M. & Zhou, H. Novel titanium-based O3-type NaTi0.5Ni0.5O2 as a cathode material for sodium ion batteries. *Chem. Commun.* **2014**, 50,457-459.

38 Yabuuchi, N., Kajiyama, M., Iwatate, J., Nishikawa, H., Hitomi, S., Okuyama, R., Usui, R., Yamada, Y. & Komaba, S. P2-type Nax[Fe1/2Mn1/2]O2 made from earth-abundant elements for rechargeable Na batteries. *Nat. Mater.* **2012**, 11,512-517.

39 Masquelier, C. & Croguennec, L. Polyanionic (Phosphates, Silicates, Sulfates) Frameworks as Electrode Materials for Rechargeable Li (or Na) Batteries. *Chem. Rev.* **2013**, 113,6552-6591.

40 Padhi, A. K., Nanjundaswamy, K. S. & Goodenough, J. B. Phospho-olivines as Positive-Electrode Materials for Rechargeable Lithium Batteries. *J. Electrochem. Soc.* **1997**, 144,1188-1194.

41 Barpanda, P., Ye, T., Nishimura, S.-i., Chung, S.-C., Yamada, Y., Okubo, M., Zhou, H. &

Yamada, A. Sodium iron pyrophosphate: A novel 3.0V iron-based cathode for sodium-ion batteries. *Electrochem. Commun.* **2012**, 24,116-119.

42 Kim, M.-J., Jeon, I.-Y., Seo, J.-M., Dai, L. & Baek, J.-B. Graphene Phosphonic Acid as an Efficient Flame Retardant. *ACS Nano* **2014**, 8,2820-2825.

43 Bu, P., Liu, S., Lu, Y., Zhuang, S., Wang, H. & Tu, F. Effects of Carbon Black on the Electrochemical Performance of Lithium-Organic Coordination Compound Batteries. *Int. J. Electrochem. Sci* **2012**, 7,4617-4624.

44 Chen, C. H., Liu, J. & Amine, K. Symmetric cell approach and impedance spectroscopy of high power lithium-ion batteries. *J. Power Sources* **2001**, 96,321-328.

45 Petibon, R., Sinha, N. N., Burns, J. C., Aiken, C. P., Ye, H., VanElzen, C. M., Jain, G., Trussler, S. & Dahn, J. R. Comparative study of electrolyte additives using electrochemical impedance spectroscopy on symmetric cells. *J. Power Sources* **2014**, 251,187-194.

46 Park, S.-J., Ryu, J.-H. & Oh, S.-M. The Roles of Electrolyte Additives on Low-temperature Performances of Graphite Negative Electrode. *J. Korean Electrochem. Soc.* **2012**, 15,19-26.

47 Delpeux, S., Beguin, F., Benoit, R., Erre, R., Manolova, N. & Rashkov, I. Fullerene core star-like polymers—1. Preparation from fullerenes and monoazidopolyethers. *Eur. Polym. J.* **1998**, 34,905-915.

48 Goldberg, M. J., Clabes, J. G. & Kovac, C. A. Metal–polymer chemistry. II. Chromium–polyimide interface reactions and related organometallic chemistry. *J. Vac. Sci. Technol., A* **1988**, 6,991-996.

49 Nesbitt, H. W., Bancroft, G. M., Henderson, G. S., Ho, R., Dalby, K. N., Huang, Y. & Yan, Z. Bridging, non-bridging and free (O^{2-}) oxygen in Na_2O-SiO_2 glasses: An X-ray Photoelectron Spectroscopic (XPS) and Nuclear Magnetic Resonance (NMR) study. *J. Non-Cryst. Solids* **2011**, 357,170-180.

50 Murakami, M., Yamashige, H., Arai, H., Uchimoto, Y. & Ogumi, Z. Direct Evidence of LiF Formation at Electrode/Electrolyte Interface by 7Li and 19F Double-Resonance Solid-State NMR Spectroscopy. *Electrochem. Solid-State Lett.* **2011**, 14,A134-A137.

51 Balasubramanian, M., Lee, H. S., Sun, X., Yang, X. Q., Moodenbaugh, A. R., McBreen, J., Fischer, D. A. & Fu, Z. Formation of SEI on Cycled Lithium-Ion Battery Cathodes: Soft X-Ray Absorption Study. *Electrochem. Solid-State Lett.* **2002**, 5,A22-A25.

52 Aurbach, D., Markovsky, B., Rodkin, A., Cojocaru, M., Levi, E. & Kim, H.-J. An analysis of rechargeable lithium-ion batteries after prolonged cycling. *Electrochim. Acta* **2002**, 47,1899-1911.